

DECELLULARIZATION OF PORCINE CARTILAGE PROMOTES
CHONDROGENIC DIFFERENTIATION OF HUMAN CHONDROCYTES

by

Roxanne Nicole Stone



A thesis

submitted in partial fulfillment

of the requirements for the degree of

Master of Science in Interdisciplinary Studies,

Biomedical Engineering and Health Science

Boise State University

August 2020

© 2020

Roxanne Nicole Stone

ALL RIGHTS RESERVED

BOISE STATE UNIVERSITY GRADUATE COLLEGE

DEFENSE COMMITTEE AND FINAL READING APPROVALS

of the thesis submitted by

Roxanne Nicole Stone

Thesis Title: Decellularization of Porcine Cartilage Promotes Chondrogenic
Differentiation of Human Chondrocytes

Date of Final Oral Examination: 29 June 2020

The following individuals read and discussed the thesis submitted by student Roxanne Nicole Stone, and they evaluated her presentation and response to questions during the final oral examination. They found that the student passed the final oral examination.

David Estrada, Ph.D. Chair, Supervisory Committee

Julia Oxford, Ph.D. Member, Supervisory Committee

Amy Moll, Ph.D. Member, Supervisory Committee

The final reading approval of the thesis was granted by David Estrada, Ph.D., Chair of the Supervisory Committee. The thesis was approved by the Graduate College.

DEDICATION

This research is dedicated to the individuals suffering from osteoarthritis. The results from this research project specifically are dedicated to all the research related to improving osteoarthritis treatment options. Let's improve health care options!

ACKNOWLEDGMENTS

I would like to express a very special thank you to my supervisor and coworkers in the College of Engineering Advising and Outreach Office, for supporting me while going to school part-time and working full time as an Academic Advisor. I would also like to acknowledge my mentors, David Estrada, Amy Moll, and Julie Oxford, who have supported me in this nontraditional master's degree.

I would additionally like to acknowledge Wakefield Meats in Melba, Idaho for providing the tissue donation, which was the foundation for this research project. Financial support was kindly provided by the Boise State University Biomolecular Research Center (P20GM109095 and P20GM103408) and Advance Nanomaterials and Manufacturing Laboratory.

ABSTRACT

Knee osteoarthritis (knee OA) is the most common type of osteoarthritis (OA) and accounts for 70% of arthritis-related hospital admissions and 23% of clinical visits. Major limitations in both the current non-surgical and surgical methods are that they only relieve pain and show no evidence for restoring natural tissue anatomy. Leaders in the field propose that a stem cell treatment approach holds promise for the regeneration of a greater proportion of hyaline-like tissue at the repair site (Cross et al., 2014; Escobar Ivirico, Bhattacharjee, Kuyinu, Nair, & Laurencin, 2017; Helmick et al., 2008; Toh, Foldager, Pei, & Hui, 2014).

It is hypothesized that the fate of cells to differentiate toward a specific lineage is governed by cell-to-cell and cell-to-matrix interactions (Djouad, Mrugala, Noël, & Jorgensen, 2006). It is necessary to continue the optimization of cell-based biomaterials for clinically relevant therapies (Gupta PK et al., 2012).

To continue improving cell therapy options applicable to knee OA, decellularized cartilage from a porcine ear was used as the scaffold for the growth and differentiation of human cartilage cells. Decellularization techniques have been used to isolate an extracellular matrix (ECM) scaffold from cells in culture, tissues, or organs. These previous methods served as the foundation for the similar procedures used in this study. Results presented by proteomic data showed that the methods used for decellularization were successful in the removal of cellular components including nuclei, mitochondria,

cytosol, rough endoplasmic reticulum, plasma membrane, and Golgi biomarkers.

Histology and scanning electron microscopy (SEM) show that decellularization resulted in creating a more porous scaffold. SEM also showed that cells adhered to the surface of this novel scaffold.

TABLE OF CONTENTS

DEDICATION	iv
ACKNOWLEDGMENTS	v
ABSTRACT.....	vi
LIST OF TABLES	x
LIST OF FIGURES	xi
LIST OF ABBREVIATIONS.....	xiii
CHAPTER ONE: INTRODUCTION.....	1
Cartilage in the Knee and Osteoarthritis.....	1
CHAPTER TWO: STEM CELL OPTIONS.....	4
CHAPTER THREE: DECELLULARIZATION AS A BIOMATERIAL	7
Decellularization Strategies	8
Determining the level of Decellularization.....	10
Recellularization of a Decellularized Scaffold	12
CHAPTER FOUR: RESEARCH MATERIALS AND METHODS.....	13
Materials	13
Dissection Methods.....	13
Decellularization Methods	14
DNA Extraction	17
Histology.....	18

Hoechst Evaluation	20
SEM Preparation and Imaging.....	20
PCR.....	21
Proteomics.....	23
Recellularization of the Decellularized Scaffold	24
CHAPTER FIVE: RESULTS AND DISCUSSION.....	26
Characterization Before and After Decellularization	27
DNA Extraction	27
Proteomic Data.....	30
Histology.....	46
Hoechst Evaluation	48
SEM Preparation and Imaging.....	49
Characterization After Recellularization	51
Histology.....	51
SEM Imaging	53
Characterization of Cellular Response to the Scaffolds	55
Q-RT-PCR	56
Markers of Chondrogenesis detected by Mass Spectrometry after growth on Decellularized Scaffold.....	63
CHAPTER SIX: CONCLUSIONS AND FUTURE WORK	64
REFERENCES	67

LIST OF TABLES

Table 1	Summary of DNA Extract showing decrease in DNA content after first wash cycle.....	28
Table 2	Summary of DNA Extract showing decrease in DNA content after final wash cycle.....	29
Table 3	Cellular proteins depleted by decellularization process.....	31
Table 4	Mitochondrial proteins depleted by decellularization process.....	33
Table 5	Cytosolic proteins depleted by decellularization process	35
Table 6	Membrane proteins depleted by decellularization process	38
Table 7	Endoplasmic reticulum depleted by decellularization process	42
Table 8	Golgi proteins depleted by decellularization process	43
Table 9	Extracellular matrix noncollagenous proteins depleted by decellularization process.....	44
Table 10	Housekeeping genes.....	56
Table 11	Chondrogenic markers expressed by chondrocytes that are enhanced by growth on the scaffold not seen on TC plastic and their function	60

LIST OF FIGURES

Figure 1	Structural Changes between a healthy knee joint and an OA knee (Horizon Pharma).....	3
Figure 2	Flowchart of Decellularization	16
Figure 3	Key to figure 2, Flowchart of Decellularization	17
Figure 4	Flowchart highlighting the steps in dehydration.....	19
Figure 5	A.) Example of how Tissue was embedded in Paraffin Wax. Orange shows transverse orientation and blue represents the cross-sectional. B.) Shows the actual tissue embedded in a thin sheet of Paraffin Wax.....	19
Figure 6	Isolated Pig Ear Cartilage	26
Figure 7	Cartilage Disk with an 8mm Diameter	26
Figure 8	A) Boise State B. B) Boise State B 8mm Diameter shape made from original isolated cartilage material.....	27
Figure 9	DNA Decrease after final wash cycle.....	29
Figure 10	Composition of cartilage before (blue) and after (red) decellularization .	45
Figure 11	H&E Stain on Non-Decellularized Cartilage. 10x Transverse Image, with a scale bar of 100 μ m	46
Figure 12	H&E Stain on Final Decellularized Cartilage. 10x Transverse Image, with a scale bar of 100 μ m	47
Figure 13	Alcian Blue Stain on Final Decellularized Cartilage. 10x Transverse Image, with a scale bar of 100 μ m	48
Figure 14	Hoechst Stain at 40x, with a scale bar of 50 μ m. A) Non-Decellularized Sample. B) Decellularized Sample	49
Figure 15	Non-Decellularized Cartilage Disk. Scale bar of 20 μ m	50

Figure 16	Final Decellularized Cartilage Disk. Scale bar of 20µm	51
Figure 17	Recellularized Boise State B Cartilage Sample with Alcian Blue Stain at 20x, with a scale bar of 50 µm	52
Figure 18	Recellularized Boise State B Cartilage Sample with H&E Stain at 20x, with a scale bar of 50 µm	53
Figure 19	Recellularized Cartilage Disk with C28/I2 Cells at week 1. Scale bar of 20µm	54
Figure 20	Recellularized Boise State B shaped Cartilage Disk with C28/I2 Cells at 8 months. Scale bar of 20µm	55
Figure 21	HPRT1 - GAPDH correlation.....	57
Figure 22	Increase in gene expression during chondrogenesis on TC plastic.....	58
Figure 23	Cartilage scaffold supports more robust gene expression than TC plastic	58
Figure 24	Percent Change of Collagen Content.....	63

LIST OF ABBREVIATIONS

OA	Osteoarthritis
Knee OA	Knee Osteoarthritis
GAGs	Glycosaminoglycans
HA	Hyaluronic Acid
ECM	Extracellular Matrix
MSC	Mesenchymal Stem Cells
DNA	Deoxyribonucleic Acid
SDS	Sodium Dodecyl Sulfate
NaOH	Sodium Hydroxide
PBS	Phosphate-Buffered Saline
DNase	Deoxyribonuclease
RNase	Ribonuclease
RNA	Ribonucleic acid
H&E	Hematoxylin and Eosin
PCR	Polymerase Chain Reaction
SEM	Scanning Electron Microscopy
M	Molarity
° C	Degrees Celsius
mm	Millimeter
L	Liter

DI	Deionized Water
mM	Millimolar
Tris	Tris(hydroxymethyl)aminomethane
nM	Nanomolar
HCl	Hydrochloric Acid
EDTA	Ethylenediaminetetraacetic Acid
MgCl ₂	Magnesium chloride
DTT	Dithiothreitol
pH	Power of Hydrogen
w/v	Weight/Volume
mL	Milliliter
U/mL	Units Per Milliliter
C28/I2	Immortalized Human Chondrocyte
DMEM	Dulbecco's Modified Eagle's medium
FBS	Fetal Bovine Serum
g	Grams or Gravity
ATL	Buffer ATL – SDS Buffer for purification
μL	Microliters
AL	Buffer AL - Guanidine Hydrochloride and Maleic acid
RPM	Revolutions Per Minute
AW1	Guanidine Solution
AW2	Tris-Ethanol Solution
AE	Buffer AE – Tris-HCl-EDTA Solution

UV-Vis	Ultraviolet-visible Spectroscopy
ng	Nanograms
PFA	Paraformaldehyde
EtOH	Ethanol
Mbar	Megabar
mA	Milliamp
kV	Kilovolts
cDNA	Complementary DNA
nm	Nanometer
RIPA	Radioimmunoprecipitation Assay
G	Gravitational Constant
Da	Dalton
FDR	False Discovery Rate
PSMs	Peptide Spectral Matches
BCA	Bicinchoninic Acid
3-D	Three-Dimensional
2-D	Two-Dimensional
TC	Tissue Culture

CHAPTER ONE: INTRODUCTION

Arthritis is defined as inflammation of the joints in the body and has several different classifications. Osteoarthritis (OA) is the most common type and is defined as a chronic, debilitating, and painful disease. It is estimated to be one of the leading causes of disability worldwide (Cross et al., 2014; Escobar Ivirico et al., 2017; Helmick et al., 2008; Toh et al., 2014).

Sports, recreational activities, and daily movements all can cause cartilage lesions. Lesions, or chondral defects, left untreated can lead to degenerative joint disease that may include an inflammatory response (Gupta PK et al., 2012; Toh et al., 2014).

Cartilage in the Knee and Osteoarthritis

Knee osteoarthritis (knee OA) is the most common type of OA and accounts for 70% of arthritis-related hospital admissions and 23% of clinical visits (Escobar Ivirico et al., 2017). Given its anatomical position the knee, acts as a shock absorber by withstanding both tension and compression (Goldberg, Mitchell, Soans, Kim, & Zaidi, 2017). Hyaline cartilage within articular joints is located at the ends of long bones. Cartilage lacks nerve fibers, is avascular, and is composed mostly of water. It is tough, yet flexible and contains large amounts of glycosaminoglycans (GAGs) such as chondroitin sulfate and hyaluronic acid (HA), electrostatically bound to type II collagen fibers. Proteoglycans, such as aggrecan, are predominant molecular constituents of articular cartilage (Cheng, Solorio, & Alsberg, 2014; Escobar Ivirico et al., 2017; Toh et al., 2014).

The precisely organized architecture of the extracellular matrix (ECM) provides the tissue's normal structural integrity. The function of the articular cartilage is to protect the subchondral bone from mechanical forces by distributing the load equally while maintaining low friction across joint surfaces (Cheng et al., 2014; Escobar Ivirico et al., 2017; Toh et al., 2014). While normal cartilage supports tissue homeostasis and chondrocytic differentiation, osteoarthritic cartilage does not effectively carry out the functions of maintaining cartilage homeostasis and cellular differentiation (Toh et al., 2014).

Chondroblasts are the predominant cell type in growing cartilage. These cells produce new ECM until the skeleton stops growing at adolescence. Mature chondrocytes rarely divide and have limited ability to proliferate. Chondrocytes have been shown to decrease with age, which may explain why cartilage lesions do not spontaneously heal (Djouad et al., 2006; Goldberg et al., 2017; Toh et al., 2014). Older adults, above the age of 50, are at an increased risk for knee OA; this is thought to be due in part to hormonal changes that cause biological aging in the chondrocytes. Research is currently underway to better understand why OA is more common in women than men (Escobar Ivirico et al., 2017).

Articular cartilage degeneration begins at the surface of the bone in the synovial joint due to the onset of fibrillation, which disrupts the molecular framework of the ECM. These changes are triggered by mechanical damage or wear and tear of the tissue. The collagen fibrils disorient beneath the surface, and a decrease in HA and aggrecan have been reported. Figure 1 highlights the anatomy and structural changes to the knee joint due to knee OA (Escobar Ivirico et al., 2017; Toh et al., 2014). The blue in the figure

represents healthy articular cartilage. The red represents progression of cartilage degradation. When the knee shows no signs of OA, it is classified as stage 0. Stage four, the final stage is the most severe type of joint damage (Escobar Ivirico et al., 2017).



Figure 1 Structural Changes between a healthy knee joint and an OA knee (Horizon Pharma)

A better understanding of the cartilage degeneration mechanism could be useful to help develop new potential treatment strategies to repair damaged cartilage. Currently, the main treatment option for knee OA is full knee replacement (Escobar Ivirico et al., 2017).

CHAPTER TWO: STEM CELL OPTIONS

Stem cells are undifferentiated, unspecialized cells that can self-renew and may give rise to one or more specialized cell types (Gupta PK et al., 2012). Cells are thought to have a common embryonic origin for cellular descendants in the human body. Each major class of connective tissue has a fundamental cell type that can exist in both a mature and an immature form (Gupta PK et al., 2012).

Mesenchymal stem cells (MSCs) are the immature form of a chondroblast which differentiates into a chondrocyte and secretes molecules that form cartilage tissue. MSCs are multipotent stem cells that can differentiate into multiple cell types. Hyaline is one of three possible cartilage subclasses: elastic, fibro-, and hyaline. MSCs have a tri-lineage differentiation capacity, including bone, cartilage, and muscle (Gupta PK et al., 2012; Olivares-Navarrete et al., 2015).

The multipotential cell capacity of MSCs has enabled doctors to explore using genetic engineering approaches to grow cartilage within a symptomatic osteochondral defect. Studies have shown how manipulation of these cells can generate a layer of hyaline cartilage (Goldberg et al., 2017). Major limitations in both the current non-surgical and surgical methods, result in relief of pain with no evidence for the restoration of natural tissue anatomy. It is proposed that an MSC treatment approach could result in a higher proportion of hyaline-like tissue at the repair site (Escobar Ivirico et al., 2017).

Researchers have developed a wide variety of optimal cell sources for repair, such as MSC harvested from bone marrow, peripheral blood, adipose tissues, muscle, dermis,

synovium, umbilical cord blood, placenta, and dental tissues (Djouad et al., 2006; Escobar Ivirico et al., 2017; Gilpin & Yang, 2017; Gupta PK et al., 2012; Toh et al., 2014). Bone marrow-derived MSCs are currently used in clinical trial applications for articular cartilage repair. This cell population has demonstrated potential for differentiation into chondrocytic cells for cartilage tissue engineering. Studies show an improved outcome in overall tissue regeneration when cell differentiation is supported, as indicated by secretion of growth factors and matrix molecules that are characteristic of cartilage tissue (Toh et al., 2014).

Once an MSC cell source is isolated, it is capable of expansion and expression of cartilage-specific molecules with or without scaffolds for successful cartilage repair. Personalized reprogramming by gene and protein factors could lead to new advances in engineering and regenerative medicine. Current techniques use biomaterials to deliver MSCs and biological signals to the defect area (Escobar Ivirico et al., 2017; Toh et al., 2014).

The major limitation in current recellularization approaches through cell therapy is the formation of fibrocartilage rather than the desired hyaline cartilage. There can also be cell retention in the target area resulting in the loss of cells, which creates the potential for cells to move to other parts of the body (Djouad et al., 2006; Escobar Ivirico et al., 2017; Goldberg et al., 2017). To avoid this issue, it is important to design advance delivery systems. Biomaterials designed to improve cell adhesion and promote differentiation that leads to healing in damaged tissue can be used as an alternative approach for cartilage lesions and OA treatment (Escobar Ivirico et al., 2017; Toh et al.,

2014). It is necessary to continue the pursuit of improving MSC use for clinically-relevant therapies (Gupta PK et al., 2012).

CHAPTER THREE: DECELLULARIZATION AS A BIOMATERIAL

It is hypothesized that the fate of stem cells as they differentiate toward specific lineage is governed by the scaffold, specific cell-to-cell and cell-to-matrix interactions (Djouad et al., 2006; Gilpin & Yang, 2017).

Many studies report the use of various scaffolds to improve maintenance of the cells inside the defect and the provision of a chondroinductive matrix (Djouad et al., 2006; Escobar Ivirico et al., 2017; Toh et al., 2014). Besides biocompatibility, the agreed upon criteria for tissue engineering composites are 1) resorbability, 2) the ability to resist mechanical stresses, and 3) clinical relevance. Data suggest that scaffolds should support cell differentiation and maintenance of a mature phenotype when combined with MSCs. The regeneration of a fully functional tissue will depend on cell density and growth factors present inside the matrix (Djouad et al., 2006).

Decellularization techniques have been used to isolate a biological ECM from cells in culture, tissues, or organs. Cellular material that could cause an adverse effect must be removed (Cheng et al., 2014; Gilpin & Yang, 2017; Toh et al., 2014).

Decellularization methods can be administered to multiple types of tissues (Heath, 2019). This study will focus on decellularization strategies for cartilage repair.

The ultimate goal of decellularization is to remove all native genetic information and cellular components from the ECM. All Deoxyribonucleic Acid (DNA) should be removed, though the structural ECM components must be maintained. A patient's own

cells can then be used to repopulate the decellularized ECM through recellularization (Gilpin & Yang, 2017).

There is no standard decellularization method; however, best practices include chemical, physical, or combinative methods (Cheng et al., 2014; Gilpin & Yang, 2017; Heath, 2019; Seon, Marjan, Anthony, & Antonios, 2019). The decellularization process removes cells and DNA from the tissue while preserving the ECM structural components. The quality of regenerated tissue for transplantation is measured by the completeness of removal of cells, total elimination of genetic material, preservation of ECM protein content, and the retention of mechanical properties of cartilage tissue (Gilpin & Yang, 2017; Xu et al., 2014). Removal of cells and genetic material is the most critical aspect of the prevention of an immune response and potential transplant rejection (Gilpin & Yang, 2017).

In this study, decellularization strategies for cartilage were evaluated based on their ability to remove DNA and other nuclear material while preserving physical and mechanical properties of the original tissue. A future goal related to this research investigation is to use cell culture methods on a decellularized matrix to create a functional tissue for implantation.

Decellularization Strategies

Decellularization is performed using chemical, physical, or combinative methods. Surfactants, acid and bases, and enzymes make up the chemical and enzymatic portion of the process. Mechanical agents are also under study to determine if they can decellularize a tissue or organ. These agents typically work by way of lysing cells through deranging

the phospholipid bilayer cell membrane. Ionic surfactants are widely used to remove cells and genetic material (Gilpin & Yang, 2017; Heath, 2019; Seon et al., 2019).

Treatments should be applied with continuous shaking (Elder, Eleswarapu, & Athanasiou, 2009; Schwarz et al., 2012; Xu et al., 2014). Sodium dodecyl sulfate (SDS) currently meets the standard requirements of complete cell removal and elimination of at least 90% DNA. SDS has been shown to damage structural properties if used at high concentration for long durations (Cheng et al., 2014; Elder et al., 2009; Gilpin & Yang, 2017; Heath, 2019). Five different decellularization treatments showed that several methods resulted in a significant reduction of DNA. Treatment with 2% SDS for eight hours resulted in the greatest decrease of DNA; with only minor decreased collagen content (Cheng et al., 2014; Elder et al., 2009).

Some conflicting information exists regarding the duration of 1% SDS washes. The time to reach desired decellularization results range from 24 hours to seven days (Gong et al., 2011; Luo, Eswaramoorthy, Mulhall, & Kelly, 2015). The overall results indicated that the number of cells could be significantly reduced from engineered constructs. Higher or lower levels of DNA most likely relates to the thickness of tissue and the concentration and duration of specific detergents (Elder et al., 2009; Luo et al., 2015).

Only a few studies have explored decellularization of whole cartilage scaffolds for joint regeneration. Cartilage is considered immunologically privileged (Luo et al., 2015; Schwarz et al., 2012). Ethanol (EtOH) can be used to defat samples. Guanidine hydrochloride and sodium acetate can be used to denature and remove noncollagenous components (Schwarz et al., 2012). Sodium Hydroxide (NaOH) is recommended to

inactivate cellular proteins, pathogens, and denature DNA and RNA. NaOH treatment removes cells and helps increase the porosity of the tissue (Luo et al., 2015; Schwarz et al., 2012).

Freeze-thaw cycles help to increase the porosity by forming more pores after ice crystal formation and by killing innate chondrocytes. These cycles are often done in phosphate-buffered saline (PBS) solution to maintain physiological pH and osmolality, which additionally helps remove the residual reagents (Cheng et al., 2014; Gilpin & Yang, 2017; Heath, 2019; Kiyotake, Beck, & Detamore, 2016; Luo et al., 2015; Peretti, Randolph, & Caruso, 1998; Vas et al., 2018; Xu et al., 2014).

Deoxyribonuclease (DNase) and ribonuclease (RNase) are used to remove DNA and Ribonucleic acid (RNA). It could take as many as three cycles to exhibit a 95% decrease in native genetic material (Elder et al., 2009; Gilpin & Yang, 2017; Luo et al., 2015; Vas et al., 2018; Xu et al., 2014). Removal of 99% of genomic information was observed after a six day wash cycle (Luo et al., 2015).

Lyophilization has also been shown to help with cell disruption and removal of cellular components. All samples should be sterilized before proceeding to cell culture (Rowland, Colucci, & Guilak, 2016; Vas et al., 2018).

Determining the level of Decellularization

Histology is the primary method used to determine if a sample has been decellularized. Hematoxylin and Eosin (H&E) staining are used to assess construct cellularity (Elder et al., 2009; Gong et al., 2011; Luo et al., 2015; Schwarz et al., 2012; Xu et al., 2014). Proteoglycans and GAG deposits can be assessed using Safranin O staining (Elder et al., 2009; Gong et al., 2011; Xu et al., 2014).

A DNA extraction process can be used to quantify the DNA present in cartilage samples before and after decellularization (Seon et al., 2019; Vas et al., 2018). The DNA content of the sample can also be measured using a Hoechst assay. DNA present within the tissue sample will be stained blue (Luo et al., 2015; Seon et al., 2019).

Polymerase chain reaction (PCR) can be used to quantify mRNA expression of key genes to evaluate the cellular differentiation of the MSCs. PCR is a technique that amplifies any nucleotide sequence and is highly sensitive to trace amounts of DNA. Therefore, chondrogenic marker genes can be analyzed for significant changes between controlled conditions (Pei, Zhang, Li, & Chen, 2012; Vas et al., 2018).

Scanning Electron Microscopy (SEM) is used to visualize the porosity and surface topology of the decellularized scaffold. SEM can also be used to compare before and after morphological changes (Gong et al., 2011; Schwarz et al., 2012; Seon et al., 2019; Xu et al., 2014).

Mass Spectrometry can be used to assess the protein content of the scaffold before and after decellularization. Additionally, proteomics can be used to monitor the response of MSCs to the decellularized tissue scaffold. There are limited proteomic studies of cartilage, which is thought to be due to the difficulty in determining the amount of protein contribution by cells relative to the total protein contributed by the ECM (Hsueh, Khabut, Kraus, Biology, & Biology, 2017).

Biomechanical testing is used on samples to monitor ultimate load, stress, and strain. Load displacement curves are considered to be a straightforward comparison of tissue strength, which is important for cartilage specimens (Elder et al., 2009; Gilpin & Yang, 2017; Gong et al., 2011; Luo et al., 2015; Schwarz et al., 2012; Xu et al., 2014).

Once a tissue sample can be confirmed as decellularized, recellularization of the scaffold can take place.

Recellularization of a Decellularized Scaffold

As described above, MSCs are seeded onto both sides of a sterile scaffold using standard cell culture techniques (Goldberg et al., 2017; Gong et al., 2011; Luo et al., 2015). Sample shapes and sizes vary in each study model. The most common diameter reported in the literature was 6-millimeter (mm). Sheets were often stacked on top of each other at different thicknesses ranging from 2 mm to 6 mm (Gong et al., 2011; Luo et al., 2015). Growth factors may be used during cell culture to improve cell differentiation (Goldberg et al., 2017; Kiyotake et al., 2016).

The time required for repopulation of scaffolds with cells varies between seven days to multiple weeks before histological analysis, SEM, biomechanical or other types of characterization testing can be used. Seeded scaffolds are commonly decellularized porcine cartilage. Animal trials are ongoing to assess the scaffold's ability to restore natural tissue anatomy. Sheets placed in animal joints are being studied to determine optimal cell density in cell culture (Cheng et al., 2014; Goldberg et al., 2017; Gong et al., 2011; Peretti et al., 1998). More work on determining cell density before implantation is recommended. Harvest from the animals typically takes place 12 weeks after implantation (Cheng et al., 2014; Gong et al., 2011; Kiyotake et al., 2016). However, a study involving mice with implanted cartilage scaffolds ranged from seven to 42 days before harvest (Kiyotake et al., 2016; Peretti et al., 1998).

CHAPTER FOUR: RESEARCH MATERIALS AND METHODS

Materials

Four pig ears were donated from Wakefield Meats in Melba, Idaho. No animals were harmed in order to perform this research. The pigs were estimated to be one year of age and adult size.

Dissection Methods

The ears were kept frozen until dissection, which took place one week after the initial donation by Wakefield Meats. The pig ears were thawed, shaved to remove hair, and then a scalpel was used to remove all remaining skin without damaging the underlying cartilage layer. Samples were placed in a 0.5 Molarity (M) NaOH bath overnight. NaOH is effective at inactivating cellular proteins and pathogens. NaOH can denature DNA and RNA, remove cells and debris, and has been shown to help increase porosity by tissue swelling (Luo et al., 2015; Schwarz et al., 2012).

Soft tissue adhering 24 hours later was removed by transfer to a 1.0 M NaOH solution for three hours followed by transfer to a 70% ethanol solution and incubated at 40 degrees Celsius (° C) on a hot plate for three hours. Ethanol was used to remove and to sterilize soft tissue (Schwarz et al., 2012).

At this time point, the four pig ear cartilage samples were converted into 8 mm circular discs. Residual decellularized material and twenty 8 mm punches were frozen to be used for characterization of the cartilage-derived scaffold before decellularization. These samples were representative of the non-decellularized material.

Decellularization Methods

The 8 mm cartilage discs underwent a decellularization cycle. A combination of methods for each wash cycle was determined by previous literature that showed effective results at removing native cells and DNA content. The first step in the decellularization process for this study was a solution containing 1 Liter (L) of Deionized Water (DI water), 1 M guanidine hydrochloride, and 0.05 M sodium acetate. Samples were incubated on a rocker at 4° C for 96 hours. This solution was used to denature and remove noncollagenous components such as GAGs (Schwarz et al., 2012).

In order to increase porosity and kill innate chondrocytes, the samples were then subjected to three freeze-thaw cycles in 1% PBS (Cheng et al., 2014; Gilpin & Yang, 2017; Kiyotake et al., 2016; Luo et al., 2015; Peretti et al., 1998; Vas et al., 2018; Xu et al., 2014).

After the third PBS freeze-thaw cycle, the samples were washed in a solution containing the following chemicals: 10 Millimolar (mM) Tris(hydroxymethyl)aminomethane (Tris), 100 Nanomolar (nM) hydrogen chloride (HCl), 2 mM Ethylenediaminetetraacetic acid (EDTA), 5 mM Magnesium chloride (MgCl₂), 100 mM Dithiothreitol (DTT), 1% SDS, and 1% Triton-X100 with a Power of Hydrogen (pH) of 8.0. This wash cycle was maintained for 39 hours and took place with agitation on a rocker at room temperature (22° C). EDTA has been shown to decrease ECM proteins (Gilpin & Yang, 2017; Luo et al., 2015; Xu et al., 2014). MgCl₂ and DTT facilitate the removal of cell membranes and antigens by increasing the solubility of proteins (Luo et al., 2015). SDS is widely used in decellularization as it alters the microstructure of protein and DNA and treatments have resulted in a significant reduction

in DNA content. SDS concentrations up to 2% Weight/Volume (w/v) have been shown to decellularize while maintaining the functional properties of tissue scaffolds (Elder et al., 2009; Gilpin & Yang, 2017; Gong et al., 2011; Luo et al., 2015; Xu et al., 2014). Triton-X100 is used for the agglutination of DNA and a decrease in GAG content. Triton-X100 is thought to be less damaging to the structure of tissues (Elder et al., 2009; Gilpin & Yang, 2017; Luo et al., 2015; Pei et al., 2012).

The third wash step was carried out to remove HA and proteoglycans inside the cartilage disk (Luo et al., 2015). This mixture consisted of PBS and 21 Units per Milliliter (U/mL) of hyaluronidase at 37° C for 24 hours.

The fourth wash step in the first round of decellularization was a combination of DNase and RNase to break down DNA and RNA (Gilpin & Yang, 2017; Luo et al., 2015). This step took place for 24 hours in an incubator held at 37° C.

At this stage, histological analysis was carried out on the non-decellularized and decellularized tissue. Residual cells were identified based on H&E staining. SEM was also done on the non-decellularized and decellularized tissues at this time point.

Another series of washes were carried out to remove the residual cells. Samples underwent another freeze-thaw cycle. Samples were allowed to swell for 30 minutes in DI water. Two percent SDS was then added to the water. Subsequently, samples were agitated for two hours at 37° C. At the end of two hours, the samples were transferred to a buffered solution of DNase for 72 hours at 37° C with agitation. Samples were analyzed by histology where cells were noted as present. Hoechst staining showed low DNA content. SEM was also done on this new sample to monitor tissue porosity.

To remove remaining cells and increase the DNA content removal, one final series of decellularization wash cycles took place. This series of wash cycles were identical to those previously described. A major difference was that these wash cycles took place under constant agitation. At the end of the final wash cycle, a 24-hour lyophilization cycle was completed. Samples at this time point represent the final decellularized material. Figure 2 is a flowchart representing a summary of the decellularization process described. Figure 3 contains information on each wash cycle.

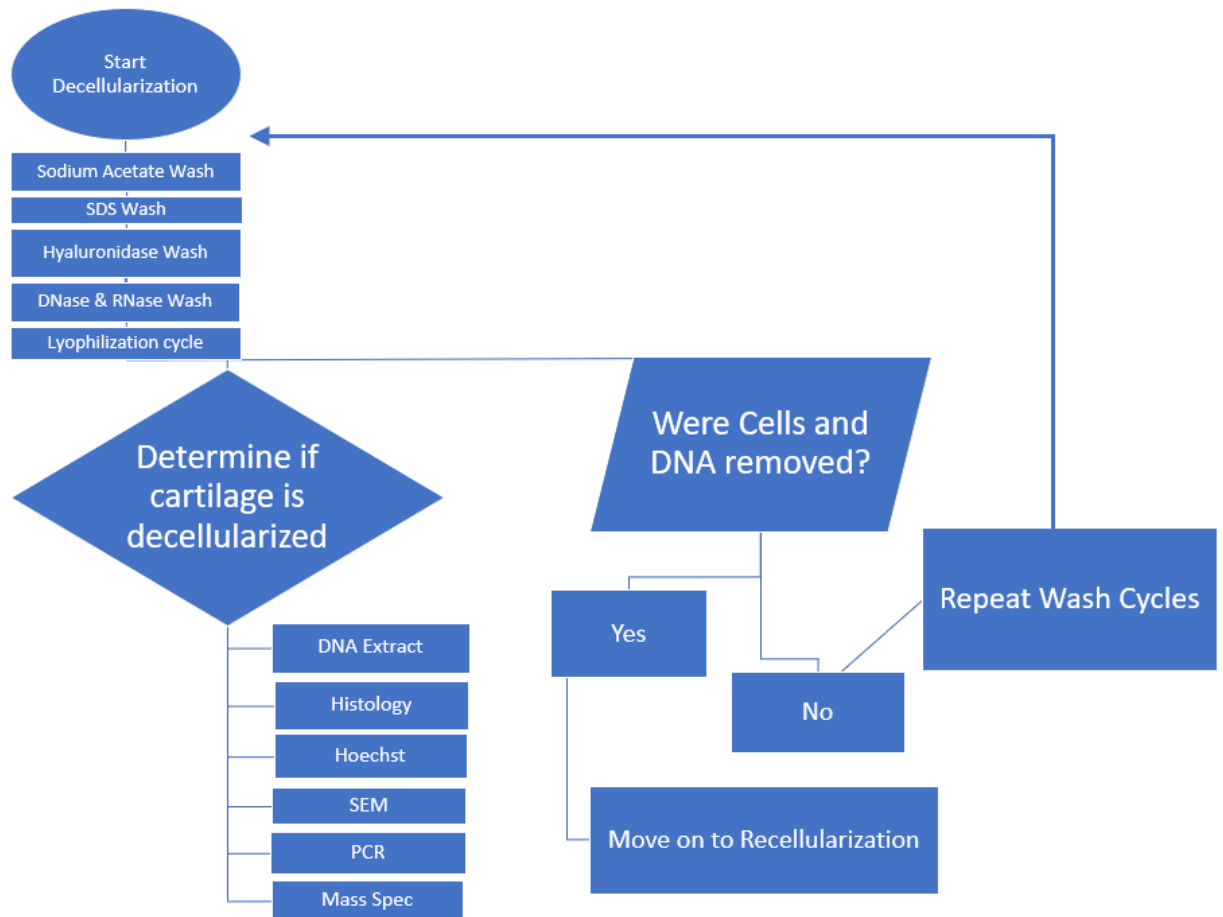


Figure 2 Flowchart of Decellularization

Key:

- Sodium Acetate and Guanidine Hydrochloride wash to denature and remove noncollagenous components with three freeze-thaw cycles to increase porosity and kill innate chondrocytes.
- SDS, Tris, HCL, EDTA, MgCl₂, DTT, Triton-X wash to decrease ECM proteins, alter microstructure of collagen fibers, and cause agglutination of DNA.
- Hyaluronidase wash to remove HA and proteoglycan inside cartilage disk.
- DNase and RNase wash to break down DNA and RNA, followed by a freeze thaw cycle to increase porosity.

Figure 3 Key to figure 2, Flowchart of DecellularizationDNA Extraction

Before moving on to recellularization, a DNA extract was done to confirm that the majority of porcine genomic DNA was removed. A total of three samples were used for both the non-decellularized material and the decellularized material. The decellularized samples were rehydrated in 10% PBS. All samples were the same weight of 0.025 grams (g). Purification of total DNA from the tissue was done with a DNeasy Kit using the protocol for purification of total DNA from animal tissues (Chomczynski 1987; Fan & Gulley, n.d.).

The tissue was cut up into small pieces and placed in 1.5 mL microcentrifuge tubes. 180 microliters (μ L) of Buffer ATL (SDS Buffer for purification) and 20 μ L of proteinase K, a broad-spectrum serine protease, was added to the tube. The tube was mixed thoroughly by vortexing. The tube was then incubated at 56°C for one hour to lyse the cells within the tissue. The tube was again vortexed for 15 seconds. 200 μ L of Buffer AL (Guanidine Hydrochloride and Maleic acid) was added to the sample and mixed thoroughly by vortexing. 200 μ L of ethanol was added to the sample and mixed by vortexing the tube. The mixture, including precipitate, was moved into the DNeasy Mini spin column using a pipette. This spin column was placed into a 2 mL collection tube and centrifuged at 8,000 revolutions per minute (rpm) for one minute. The flow-through and collection tube was discarded. The DNeasy Mini spin column was placed into a new 2

mL collection tube. 500 μ L of Buffer AW1 (Guanidine Solution) was added to the sample and was centrifuged for one minute at 8,000 rpm. The flow-through and collection tube was again discarded. The DNeasy Mini spin column was placed into a new 2 mL collection tube. 500 μ L of Buffer AW2 (Tris-Ethanol Solution) was added to the sample and was centrifuged for three minutes at 14,000 rpm to dry the DNeasy membrane. The DNeasy spin column was placed in a clean 1.5 mL microcentrifuge tube. 200 μ L of Buffer AE (10mM Tris-HCl and 0.5 mM EDTA, pH 9.0) was added to the sample. The sample was incubated at room temperature for one minute, then centrifuged for one minute at 8,000 rpm to elute.

Histology

To visualize the microscopic anatomy of cells and tissues, histology was used. The cartilage samples were fixed by soaking in 4% paraformaldehyde (PFA) for one hour then stored in 35% ethanol at 4° C until further processing. Histological processing consisted of a dehydration embedding program that was 105 minutes. The embedding process had, as outlined in figure 4, 12 stations. The first seven stations were ethanol stations at various percentages. Step eight was a 1:1 EtOH:Histoclear station. Stations nine and ten were 100% Histoclear, followed by stations 11 and 12, which were 100% paraffin wax.



Figure 4 Flowchart highlighting the steps in dehydration

After dehydration, the tissue was cut in half and embedded into a block. Figure 5 shows half the tissue placed in a transverse orientation, represented in orange. The other half was placed in a cross-sectional orientation, represented in blue.

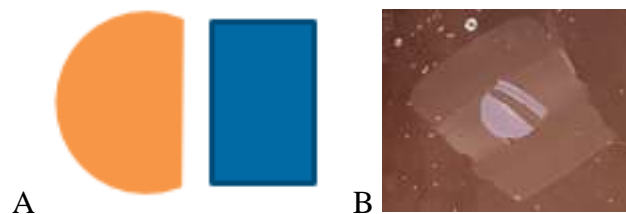


Figure 5 A.) Example of how Tissue was embedded in Paraffin Wax. Orange shows transverse orientation and blue represents the cross-sectional. B.) Shows the actual tissue embedded in a thin sheet of Paraffin Wax

Figure 5B shows a block sectioned with a sample in transverse and cross-sectional configuration on a microscope slide. After the slide was prepared, it was stained with H&E or Alcian Blue. H&E staining detected nucleic acids and endoplasmic reticulum, indicated by blue stain; and elastic, collagen, and reticular fibers indicated by pink staining. Alcian Blue is commonly used with cartilaginous tissue as it stains acidic polysaccharides, such as glycosaminoglycans, and results in a bright greenish-blue color.

Hoechst Evaluation

A slide created from the histology steps described above was dewaxed and hydrated. After this step, the slide only contained a tissue sample adhered to a glass slide. This sample was stained with Hoechst stain. Hoechst stain is specific for DNA and results in a blue stain. A total of 1 $\mu\text{g}/\text{mL}$ of Hoechst stain was placed on the sample for five minutes; it was then rinsed three times with PBS. The samples were imaged on a Zeiss Confocal LSM 510 Meta microscope.

SEM Preparation and Imaging

All cartilage disks were soaked in 4% PFA for one hour and stored in 35% ethanol at 4°C until further SEM processing. Samples were then fixed in 2.5% glutaraldehyde and 1% osmium tetroxide in Nanopure water. After fixation, they were rinsed in Nanopure water and underwent a dehydration sequence with 50%, 70%, 90% and 100% ethanol. Critical point drying was performed for ten cycles at 5 °C then allowed to heat up to 35 °C. Samples were positioned onto an aluminum stub and sealed by vacuum. Gold sputtering was performed at 0.15 millibar (mbar) and 10 milliamps (mA) for 15 cycles; 60 seconds sputtering and 60 seconds of rest. Prepped samples were

examined at an accelerating voltage of 15 kilovolts (kV) using the secondary electron detector.

PCR

Two cartilage disks were put in 1mL of Trizol and homogenized using an OMNI International TH homogenizer. A total of three test tubes, with two cartilage disks per-tube, were used. The TRIZol Reagent Isolate DNA procedure was completed before moving on to the protocol for complementary DNA (cDNA) synthesis using the RT² First Strand Kit (RT-RealTime).

The sample was centrifuged for five minutes at 12,000 x g at 4 °C. The clear supernatant was put in a new tube and incubated for five minutes. The sample was incubated for an additional two minutes after adding 0.2 mL of Chloroform to the tube. The sample was then centrifuged for 15 minutes at 12,000 x g at 4 °C. The aqueous phase containing the RNA was transferred to a new tube.

To continue isolating the RNA, 0.5 mL of Isopropanol was added to the aqueous phase and incubated for ten minutes. The sample was then centrifuged for ten minutes at 12,000 x g at 4 °C (Qiagen, 2020). At this stage, the supernatant was removed. The pellet was resuspended in 1 mL of 75% ethanol, vortexed briefly, then centrifuged for five minutes at 7,500 x g at 4 °C. The supernatant was removed, and the pellet was left to air dry. Once dry, the pellet was resuspended in 20 µL of RNase-free water and 0.1 mM EDTA. It was then incubated in a heated block at 55 °C for ten minutes.

At this stage, the DNA yield was determined by measuring the absorbance at 260 nanometers (nm) and 280 nm as described in the protocol for “Purification of Total DNA from Animal Tissue.” The next step was to follow the protocol for cDNA synthesis using

the RT² First Strand Kit. A genomic DNA elimination mix was created using 1.5 μ L of RNA, 2 μ L of Buffer GE, and 6.5 μ L RNase-free water. This mix was incubated for five minutes at 42 °C and placed immediately on ice for one minute. A reverse-transcription mix was created using 4 μ L of 5x Buffer BC3, 1 μ L Control P2, 2 μ L RE3 Reverse Transcriptase Mix, and 3 μ L RNase-free water. The 10 μ L reverse-transcription mix was added to the genomic DNA elimination mix and mixed gently by pipetting up and down. This mixture was incubated for 15 minutes at 42 °C and then 95 °C for five minutes. At this stage, 91 μ L of RNase-free water was added to the reaction and the Real-Time PCR array format followed was format F for a 96-well plate.

Following format F instructions, the PCR components mix was 1350 μ L of 2x RT² SYBR Green Mastermix, 102 μ L of cDNA synthesis reaction, and 1248 μ L of RNase-free water. This PCR components mix was loaded into a 96-well plate, 25 μ L of PCR components mix was added to each well using an eight-channel pipettor. Once filled, the plate was tightly sealed with an adhesive film. The plate was centrifuged for one minute at 1000 x g at room temperature to remove bubbles. The real-time cycler was programmed for Roche LightCycler96® conditions. The sample underwent one cycle for ten minutes at 95 °C and then 45 cycles of 15 seconds at 95 °C and one minute of 60 °C. Genes analyzed included extracellular matrix proteins, matrix remodeling enzymes, and cell adhesion molecules. Relative gene expression levels, found by mean plus/minus standard deviation, were expressed with respect to housekeeping genes determined empirically for this study.

Statistical Analysis

Selection of housekeeping genes for qRT-PCR was based on pairwise analysis of variance for differences between cycle threshold values for five candidate housekeeping genes from 15 samples within this study. Additionally, correlation analysis was carried out, data was fit to a trend line, and R^2 was determined. Relative expression of genes of interest was analyzed relative to average values for GAPDH and HPRT, and expressed as mean plus/minus standard deviation. Log transformed gene expression data was subject to a paired T-test to determine if the differences in mean values for relative gene expression were statistically significant, setting significance at $p < 0.05$.

Proteomics

Two cartilage disks were put in 2 mL of RIPA (Radioimmunoprecipitation assay) buffer and then homogenized. A total of three test tubes, with two cartilage disks per-tube, were used for statistical relevance. The samples were then centrifuged at 14,000 x g for 15 minutes at 4 °C. The lysate and pellet were separated. The lysate was put in a fresh test tube and frozen at -80 °C until further processing.

Proteins from nondecellularized, decellularized, and recellularized scaffolds were extracted using the RIPA buffer protocol (Millipore, Billerica, MA).

BCA Curve

The total protein concentration of the lysate for all samples was determined via Pierce™ BCA (Bicinchoninic Acid) Protein Assay Kit, Thermo Scientific®. This is a common method to determine total protein concentration. Once total protein concentration was determined, samples were submitted for Mass Spectrometry analysis.

Mass Spectrometry

Twenty micrograms of total protein from each sample were digested with Trypsin/Lys C mix (Promega, Madison, WI) following the manufacturer's instruction. Resulting peptide mixtures were chromatographically separated on a reverse-phase C18 column (10cm x 75 μ m, 3 μ m, 120 Å) and analyzed on a Velos Pro Dual-Pressure Linear Ion Trap mass spectrometer (Thermo Fisher Scientific).

Peptide spectral matching for porcine and human protein identification were achieved by database search using Sequest HT algorithms in a Proteome Discoverer 1.4 (Thermo Fisher Scientific). Raw spectrum data were searched against the UniProtKB/Swiss-Prot protein database for mouse (May 25, 2019). The main search parameters included: trypsin, maximum missed cleavage site of two, precursor mass tolerance of 1.5 Da, fragment mass tolerance of 0.8 Da, and variable modification of oxidation/hydroxylation of methionine, proline, and lysine (+15.995Da). A decoy database search was performed to calculate a false discovery rate (FDR). Proteins containing one or more peptides with $FDR \leq 0.05$ were considered positively identified and reported. For all proteins, the total number of peptide spectral matches (PSMs) reported by the Protein Discoverer 1.4 was used for quantification. To identify newly synthesized human proteins, the number of PSMs from unique peptides for human proteins were used for quantification. The mass spectrometry analysis used three samples at each condition and time point.

Recellularization of the Decellularized Scaffold

Before starting cell culture, the final decellularized cartilage material was rehydrated in 10% PBS. Once rehydrated, the samples were sanitized by soaking in 70%

ethanol for 20 minutes. Samples were rinsed three times with PBS and then stored in PBS for 24 hours at 4 °C. The samples were then put into C28/I2 (Immortalized Human Chondrocyte) growth media, Dulbecco's Modified Eagle's medium (DMEM) with 10% Fetal Bovine Serum (FBS) and 1% P/S (penicillin-streptomycin), and stored at 4 °C for 48 hours.

Three 24-well plates were prepared by putting 300 μ L of agarose gel at the bottom of each well to encourage cell adhesion to the decellularized scaffolds. A total of 60 decellularized disks, and four Boise State B shaped cartilage scaffolds were seeded with 500,000 C28/I2 prechondrocytic mesenchymal stem cells.

C28/I2 cells were put into five tissue culture flasks, and allowed to reach 90% confluency before seeding onto the scaffolds over ten days of growth. Time points for characterization took place at one, two, and three weeks. Four samples were collected at each time point. Samples were incubated in the 24-well plates.

At 48 hours, 500 mL of fresh C28/I2 media was added to each well containing a sample. On day four, the samples were transferred to new 24-well plates containing the same amount of agarose gel at the bottom. Samples were kept flat during transfer, and 1000 mL of fresh media was added.

At one week, 1 mL of media and 20 samples were characterized. Subsequent samples were collected at weeks two and three. The Boise State B scaffolds were incubated for eight months. Throughout all incubation periods, the media was monitored and replaced when necessary.

CHAPTER FIVE: RESULTS AND DISCUSSION

At the end of the ethanol wash during the dissection stage, the cartilage was considered fully isolated, as shown in figure 6.



Figure 6 Isolated Pig Ear Cartilage

At this time point, the four pig ear cartilage samples were converted into 8 mm circular punches, as shown in figure 7. The samples were measured in thickness with a range of 1.44 mm to .74 mm; the average thickness was determined to be 1.08 mm.



Figure 7 Cartilage Disk with an 8mm Diameter

To show that these cartilage scaffolds can be made at any size and shape for patient-specific treatment options, samples were also made into the Boise State University B as shown in figure 8.

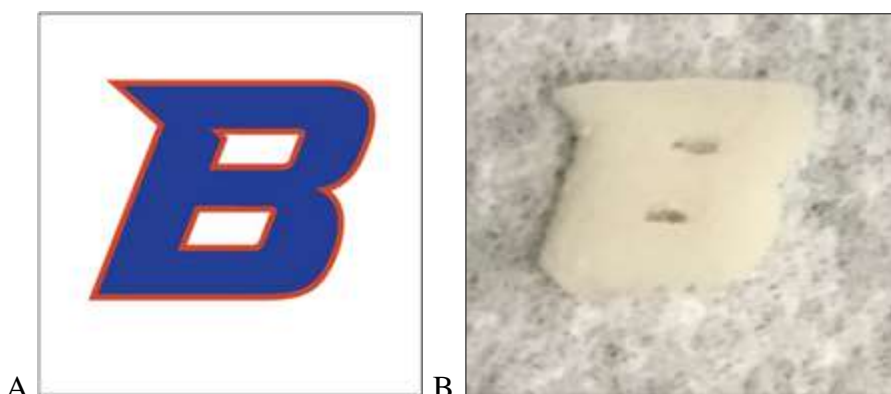


Figure 8 A) Boise State B. B) Boise State B 8mm Diameter shape made from original isolated cartilage material

Characterization Before and After Decellularization

DNA Extraction

To confirm that the majority of porcine genomic DNA was removed, genomic DNA was isolated from the cartilage disks. A total of three samples were used for both the non-decellularized material and the decellularized material. Purification of total DNA from the tissue was done using a DNeasy Kit. The protocol used was “Purification of Total DNA from Animal Tissues” as described in the methods section.

Results from this protocol were obtained by UV-Vis spectroscopy (Nanodrop spectrometer).

At the end of the first wash cycle, a DNA extract was completed. After calculating the average of nucleic acid concentration between the three samples, a 75%

decrease in DNA content using nanograms (ng) per μL was determined as outlined in table 1.

Table 1 Summary of DNA Extract showing decrease in DNA content after first wash cycle

Sample	Nucleic Acid	Unit	Sample Type
Non-decellularized material 1	991.8	ng/ μl	DNA
Non-decellularized material 2	2974.2	ng/ μl	DNA
Non-decellularized material 3	1498.3	ng/ μl	DNA
Final decellularized material 1	280.4	ng/ μl	DNA
Final decellularized material 2	592.8	ng/ μl	DNA
Final decellularized material 3	479.5	ng/ μl	DNA
Average non-decellularized material	1821.43	ng/ μl	DNA
Average final decellularized material	450.9	ng/ μl	DNA
Decrease in DNA content	75%	-	DNA

Due to the 75% initial DNA content decrease, it was decided to repeat the wash cycles using a more aggressive approach. At the end of the final wash cycle, another DNA extract using the same methods was performed. After calculating the average of nucleic acid concentration between the three samples, a 92% decrease in DNA content using nanograms (ng) per μL was determined as outlined in table 2.

Table 2 Summary of DNA Extract showing decrease in DNA content after final wash cycle

Sample	Nucleic Acid	Unit	Sample Type
Non-decellularized material 1	33.5	ng/ μ L	DNA
Non-decellularized material 2	38.7	ng/ μ L	DNA
Non-decellularized material 3	71.7	ng/ μ L	DNA
Final decellularized material 1	6.5	ng/ μ L	DNA
Final decellularized material 2	3.4	ng/ μ L	DNA
Final decellularized material 3	2.1	ng/ μ L	DNA
Average non-decellularized material	47.97	ng/ μ L	DNA
Average final decellularized material	4	ng/ μ L	DNA
Decrease in DNA content	92%	-	DNA

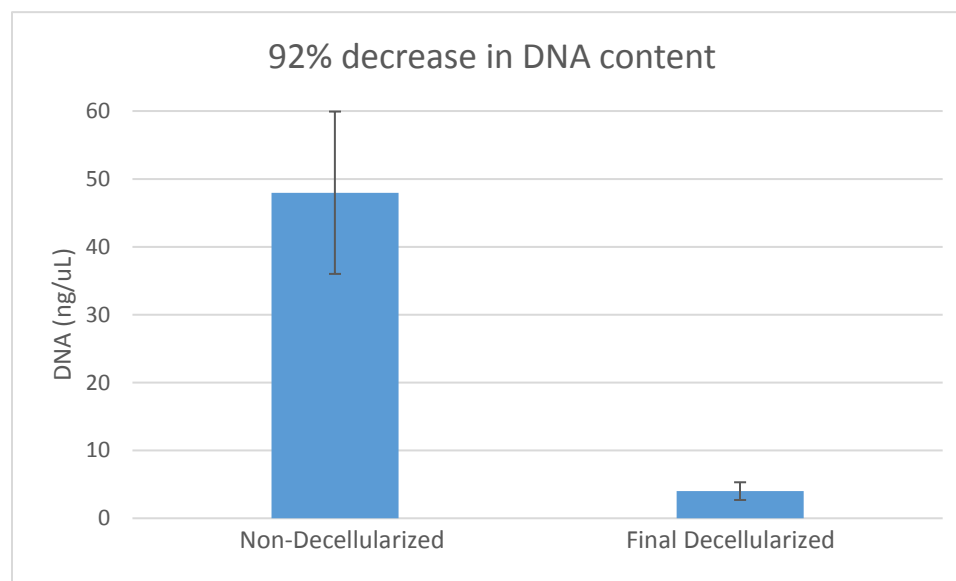


Figure 9 DNA Decrease after final wash cycle

Figure 9 shows the DNA content before and after the decellularization process. DNA was extracted and quantified spectrophotometrically. Quantitative measurements of DNA within scaffolds before and after the decellularization process indicated that residual DNA was at approximately 8% of the original content. Error bars: Mean +/- standard error of the mean, N=6.

Proteomic Data

The scaffold was also confirmed to be decellularized using Proteomic data. Several proteins were present in the non-decellularized scaffold that were not present, or were depleted by a significant amount in the decellularized scaffold. Removal of cellular components including nuclei, mitochondria, cytosol, rough endoplasmic reticulum, plasma membrane and Golgi was measured. Depletion is shown for biomarkers in tables 3 through table 8.

Table 3 Cellular proteins depleted by decellularization process

Cellular proteins depleted by decellularization process (nucleus)	% depletion	Gene symbol
Aprataxin	100	APTX
BRCA1-A complex subunit RAP80	100	UIMC1
Doublesex- and mab-3-related transcription factor 1	100	DMRT1
Histone H3.3	100	H3F3A
Interferon-induced GTP-binding protein Mx1	100	MX1
Interferon-stimulated gene 20 kDa protein	100	Isg20
Iron-responsive element-binding protein 2	100	IREB2
Myocardin	100	MYOCD
Nuclear factor of activated T-cells, cytoplasmic 1	100	NFATC1
Nuclear receptor subfamily 0 group B member 1	100	NR0B1
Polypyrimidine tract-binding protein 1	100	PTBP1
POU domain, class 5, transcription factor 1	100	POU5F1
Sorbin and SH3 domain-containing protein 2	100	SORBS2
SRSF protein kinase 3	100	SRPK3
Sterol regulatory element-binding protein 1	100	SREBF1
Histone H4	96	Histone H4
Signal transducer and activator of transcription 5A	89	STAT5A
Hepatocyte nuclear factor 1-beta	85	HNF1B
Pre-mRNA-splicing factor ATP-dependent RNA helicase DHX16	85	DHX16
V(D)J recombination-activating protein 1	83	RAG1

It was anticipated to obtain 100% removal of DNA after the decellularization treatment. It was surprising this was not the case. Even after the procedure was repeated it did not reduce the DNA content to zero percent. Additional characterization using mass spectrometry to analyze the content of the scaffold before and after treatment of decellularization was carried out. Nuclear proteins were considered potential suitable biomarkers for decellularization. A profile of 20 nuclear proteins was investigated that included APTX, UIMC1, DMRT1, H3F3A, MX1, ISG20, IREB2, MYOCD, NFATC1, NROB1, PTBP1, POU5F, SORBS2, SRPK3, SREBF1, HISTONE H4, STAT5A, HNF1B, DHX16, and RAG1. Of these, 15 were depleted to a level that rendered them no longer detectable by mass spectrometry. Five of these (HISTONE H4, STAT5A, HNF1B, DHX16, and RAG1) were depleted by 83 – 96%, indicating that there may be biochemical interactions mediating molecular interactions independent of the cellular compartment. This study has identified a nuclear protein profile of 15 proteins that could be used in the future to assess the efficiency of the decellularization process. The nuclear proteins comprising this profile are listed in table 3.

Table 4 Mitochondrial proteins depleted by decellularization process

Mitochondrial proteins	% depletion	Gene symbol
Aconitate hydratase, mitochondrial	100	ACO2
A-kinase anchor protein 10, mitochondrial	100	AKAP10
Aspartate aminotransferase, mitochondrial	100	GOT2
Carnitine O-palmitoyltransferase 1, muscle isoform	100	CPT1B
Cholesterol side-chain cleavage enzyme, mitochondrial	100	CYP11A1
Cysteine protease ATG4D	100	ATG4D
Cytochrome b-245 heavy chain	100	CYBB
Cytochrome c oxidase copper chaperone	100	COX17
Cytochrome P450 11B1, mitochondrial	100	CYP11B1
Glycerol-3-phosphate acyltransferase 1, mitochondrial	100	GPAM
Glycine amidinotransferase, mitochondrial	100	GATM
Methylmalonyl-CoA mutase, mitochondrial	100	MUT
Mitochondrial Rho GTPase 2	100	RHOT2
Mitochondrial uncoupling protein 2	100	UCP2
Mitochondrial uncoupling protein 3	100	UCP3
NADH-ubiquinone oxidoreductase chain 5	100	MT-ND5
Succinate dehydrogenase [ubiquinone] flavoprotein subunit, mitochondrial	100	SDHA
Succinate--CoA ligase [ADP/GDP-forming] subunit alpha, mitochondrial	100	SUCLG1
Valine--tRNA ligase, mitochondrial	100	VAR2
Amine oxidase [flavin-containing] B	91	MAOB
Mitochondria-eating protein	91	SPATA18

Nicotinamide phosphoribosyltransferase	91	NAMPT
Hexokinase-2 OS=Sus scrofa	87	HK2
Kynurenine 3-monooxygenase	85	KMO
NADP-dependent malic enzyme	83	ME1
Cytochrome P450 3A29	78	CYP3A29
Glyceraldehyde-3-phosphate dehydrogenase	66	GAPDH
Hydroxymethylglutaryl-CoA synthase, mitochondrial	66	HMGCS2
Creatine kinase U-type, mitochondrial	55	CKMT1

Mitochondrial proteins were also investigated to determine a protein profile of mitochondrial biomarkers that may serve as a reference set to provide more reliable indicators of decellularization. The protein content of 29 mitochondrial proteins was measured, and 19 of these (ACO2, AKAP10, GOT2, CPT1B, CYP11A1, ATC4D, CYBB, COX17, CYP11B1, GPAM, GATM, MUT, RHOT2, UCP2, UCP3, MT-ND5, SDHA, CUCLG1, and VARS2) were efficiently depleted through the decellularization process. In contrast, some mitochondrial proteins were detected after the decellularization process, indicating that they may not be reliable indicators of decellularization. Mitochondrial proteins and their extent of depletion are listed in table 4.

Table 5 Cytosolic proteins depleted by decellularization process

Cytosolic proteins	% depletion	Gene symbol
1-acylglycerol-3-phosphate O-acyltransferase ABHD5	100	ABHD5
4-hydroxyphenylpyruvate dioxygenase	100	HPD
Actin, cytoplasmic 1	100	ACTB
Alcohol dehydrogenase [NADP(+)]	100	AKR1A1
Antileukoproteinase	100	SLPI
ATP-dependent 6-phosphofructokinase, muscle type	100	PFKM
Autophagy protein 5	100	ATG5
Bifunctional epoxide hydrolase 2	100	EPHX2
Biogenesis of lysosome-related organelles complex 1 subunit 5	100	BLOC1S5
Calponin-1 OS	100	CNN1
Calponin-2	100	CNN2
Cas scaffolding protein family member 4	100	CASS4
Coatomer subunit beta	100	COPB1
Diacylglycerol kinase alpha	100	DGKA
Dihydropyrimidine dehydrogenase [NADP(+)]	100	DPYD
FAST kinase domain-containing protein 4	100	TBRG4
Gastrotropin	100	FABP6
Growth factor receptor-bound protein 10	100	Grb10
Integrin beta-1-binding protein 2	100	ITGB1BP2
L-dopachrome tautomerase	100	DCT

L-lactate dehydrogenase A chain	100	LDHA
Myosin light chain 4	100	MYL4
Myosin-1	100	MYH1
Myosin-2	100	MYH2
Nucleoside diphosphate kinase B	100	NME2
Perilipin-3	100	PLIN3
Phosphatidylinositol 4,5-bisphosphate 3-kinase catalytic subunit gamma isoform	100	PIK3CG
Serine/threonine-protein phosphatase 2A 65 kDa regulatory subunit A beta isoform	100	PPP2R1 B
Suppressor of cytokine signaling 2	100	SOCS2
Thimet oligopeptidase	100	THOP1
Triosephosphate isomerase	100	TPI1
Tubulin alpha-1A chain	100	TUBA1 A
Tubulin beta chain	100	TUBB
Vinculin	100	VCL
Serine/threonine-protein kinase WNK1	95	WNK1
L-lactate dehydrogenase B chain	94	LDHB
UTP--glucose-1-phosphate uridylyltransferase	92	UGP2
Eukaryotic initiation factor 4A-III	89	EIF4A3
Triokinase/FMN cyclase	85	TKFC
Acylphosphatase-1	83	ACYP1
Glycine N-methyltransferase	78	GNMT
N-acetylneuraminase lyase	78	NPL
Phosphatidylinositol 3-kinase catalytic subunit type 3	78	PIK3C3

Serine/threonine-protein phosphatase 1 regulatory subunit 10	64	PPP1R1 0
--	----	-------------

Cytosolic proteins were also investigated to determine a protein profile of cytosolic biomarkers that may serve as a reference set to provide further reliable indicators of decellularization. The protein content of 44 cytosolic proteins was measured, and 34 of these (ABHD5, HPD, ACTB, AKR1A1, SLPI, PFKM, ATG5, EPHX2, BLOC1S5, CNN1, CNN2, CASS4, COPB1, DGKA, DPYD, TBRG4, FABP6, Grb10, ITGB1BP2, DCT, LDHA, MYL4, MYH1, MYH2, NME2, PLIN3, PIK3CG, PPP2R1B, SOCS2, THOP1, TPI1, TUBA1A, TUBB, and VCL) were efficiently depleted through the decellularization process. In contrast, some cytosolic proteins were detected after the decellularization process, indicating that they may not be reliable indicators of decellularization. Cytosolic proteins and their extent of depletion are listed in table 5.

A total of 65 membrane proteins were investigated to analyze the extent to which they were depleted during the decellularization process. Of these, 38 membrane proteins (ARF6, ALOX15, CAPN1, CXCR4, CYSLTR2, DSG1, EDNRA, GJA1, RABGGTA, GGT1, GHR, GNAQ, ITGB1, IFNAR1, IL4R, IL6R, LDLR, KIT, STEAP1, NTRK3, PTH1R, PDZD11, ATP2B1, PECAM1, PCDH11X, RAMP1, SAG, SIGLEC1, SLA-DQCA, SLA-DQCB, SLA-DQDB, KCNN3, SLC5A1, SLC22A6, SLC22A7, TPO, TLR9, and TGFBR3) were determined to serve as reliable indicators of decellularization. Membrane protein biomarkers that may serve as suitable indicators of cellular depletion are listed in table 6.

Table 6 Membrane proteins depleted by decellularization process

Membrane proteins	% depletion	Gene symbol
ADP-ribosylation factor 6	100	ARF6
Arachidonate 15-lipoxygenase	100	ALOX15
Calpain-1 catalytic subunit	100	CAPN1
C-X-C chemokine receptor type 4	100	CXCR4
Cysteinyl leukotriene receptor 2	100	CYSLTR2
Desmoglein-1	100	DSG1
Endothelin-1 receptor	100	EDNRA
Gap junction alpha-1 protein	100	GJA1
Geranylgeranyl transferase type-2 subunit alpha	100	RABGGTA
Glutathione hydrolase 1 proenzyme	100	GGT1
Growth hormone receptor	100	GHR
Guanine nucleotide-binding protein G(q) subunit alpha	100	GNAQ
Integrin beta-1	100	ITGB1
Interferon alpha/beta receptor 1	100	IFNAR1
Interleukin-4 receptor subunit alpha	100	IL4R
Interleukin-6 receptor subunit alpha	100	IL6R
Low-density lipoprotein receptor	100	LDLR
Mast/stem cell growth factor receptor Kit	100	KIT
Metalloreductase STEAP1	100	STEAP1
NT-3 growth factor receptor	100	NTRK3
Parathyroid hormone/parathyroid hormone-related peptide receptor	100	PTH1R

PDZ domain-containing protein 11	100	PDZD11
Plasma membrane calcium-transporting ATPase 1	100	ATP2B1
Platelet endothelial cell adhesion molecule	100	PECAM1
Protocadherin-11 X-linked	100	PCDH11X
Receptor activity-modifying protein 1	100	RAMP1
S-arrestin	100	SAG
Sialoadhesin	100	SIGLEC1
SLA class II histocompatibility antigen, DQ haplotype C alpha chain	100	SLA-DQCA
SLA class II histocompatibility antigen, DQ haplotype C beta chain	100	SLA-DQCB
SLA class II histocompatibility antigen, DQ haplotype D beta chain	100	SLA-DQDB
Small conductance calcium-activated potassium channel protein 3	100	KCNN3
Sodium/glucose cotransporter 1	100	SLC5A1
Solute carrier family 22 member 6	100	SLC22A6
Solute carrier family 22 member 7	100	SLC22A7
Thyroid peroxidase	100	TPO
Toll-like receptor 9	100	TLR9
Transforming growth factor beta receptor type 3	100	TGFBR3
Beta-1 adrenergic receptor	94	ADRB1
Zonadhesin	94	ZAN
Glutathione S-transferase alpha M14	94	GSTAM14
Activin receptor type-2B	93	ACVR2B
Solute carrier family 22 member 1	91	SLC22A1
Low-density lipoprotein receptor-related protein 2	89	LRP2

Orexin receptor type 2	89	HCRTR2
Glutamate decarboxylase 2	89	GAD2
Ectonucleotide pyrophosphatase/phosphodiesterase family member 6	85	ENPP6
Tyrosine-protein kinase SYK	85	SYK
Hormone-sensitive lipase	85	LIPE
V-type proton ATPase catalytic subunit A	85	ATP6V1A
Potassium-transporting ATPase alpha chain 1	82	ATP4A
Electrogenic sodium bicarbonate cotransporter 1	81	SLC4A4
Alpha-2A adrenergic receptor	78	ADRA2A
Calcium-activated chloride channel regulator 1	78	CLCA1
Gastrin/cholecystokinin type B receptor	78	CCKBR
Hepatocyte growth factor receptor	78	MET
Leptin receptor	78	LEPR
Extracellular calcium-sensing receptor	70	CASR
Scavenger receptor class B member 1	70	SCARB1
ATP-binding cassette sub-family G member 2	66	ABCG2
Major facilitator superfamily domain-containing protein 6	66	MFSD6
H(+)/Cl(-) exchange transporter 5	63	CLCN5
Prolactin receptor	55	PRLR
Beta-3 adrenergic receptor	55	ADRB3
Lutropin-choriogonadotropic hormone receptor	55	LHCGR

Endoplasmic reticulum proteins were investigated by mass spectrometry before and after decellularization. A protein profile comprising 16 endoplasmic reticulum

proteins may be considered as reliable biomarkers for the decellularization process (RPS13, RPS3, CYP8B1, RPL14, RPL6, CRYBB1, RPN2, HSPA5, FOLH1, HSPA1A, HSPA1B, HSPA1L, HMOX1, GANAB, ATP2A2, and VCP). Mass spectrometry detected other endoplasmic reticulum proteins that were not as efficiently removed from tissue by the decellularization process. These may indicate non-specific interactions and render them as unreliable indicators of decellularization. Endoplasmic reticulum proteins and the extent to which they were depleted during the decellularization process are listed in table 7.

Table 7 Endoplasmic reticulum depleted by decellularization process

Endoplasmic reticulum	% depletion	Gene symbol
40S ribosomal protein S13	100	RPS13
40S ribosomal protein S3	100	RPS3
5-beta-cholestane-3-alpha,7-alpha-diol 12-alpha-hydroxylase	100	CYP8B1
60S ribosomal protein L14	100	RPL14
60S ribosomal protein L6	100	RPL6
Beta-crystallin B1	100	CRYBB1
Dolichyl-diphosphooligosaccharide--protein glycosyltransferase subunit 2	100	RPN2
Endoplasmic reticulum chaperone BiP	100	HSPA5
Glutamate carboxypeptidase 2	100	FOLH1
Heat shock 70 kDa protein 1A	100	HSPA1A
Heat shock 70 kDa protein 1B	100	HSPA1B
Heat shock 70 kDa protein 1-like	100	HSPA1L
Heme oxygenase 1	100	HMOX1
Neutral alpha-glucosidase AB	100	GANAB
Sarcoplasmic/endoplasmic reticulum calcium ATPase 2	100	ATP2A2
Transitional endoplasmic reticulum ATPase	100	VCP
Microsomal triglyceride transfer protein large subunit	85	MTTP
Dolichyl-diphosphooligosaccharide--protein glycosyltransferase subunit 1	78	RPN1
Dual oxidase 1	78	DUOX1
Heat shock protein HSP 90-alpha	78	HSP90AA1

Organelle cellular proteins were also analyzed, including those associated with mitochondria, Golgi, and endoplasmic reticulum. Five Golgi-specific proteins, 29 mitochondrial proteins, and 20 endoplasmic reticulum proteins were depleted as a result of the decellularization process. It was determined that Golgi proteins B3GALNT1, MAN1A1, FUT2, and MGAT4C represent a protein profile that may be suitable to monitor cellular depletion during decellularization processes. However, the Golgi protein B3GNT5 was not fully depleted in this experiment, potentially due to secondary interactions. Golgi proteins and the extent to which depletion was observed are listed in table 8.

Table 8 Golgi proteins depleted by decellularization process

Golgi	% depletion	Gene symbol
UDP-GalNAc:beta-1,3-N-acetylgalactosaminyltransferase 1	100	B3GALNT1
Mannosyl-oligosaccharide 1,2-alpha-mannosidase IA	100	MAN1A1
Galactoside 2-alpha-L-fucosyltransferase 2	100	FUT2
Alpha-1,3-mannosyl-glycoprotein 4-beta-N-acetylglucosaminyltransferase C	100	MGAT4C
Lactosylceramide 1,3-N-acetyl-beta-D-glucosaminyltransferase	66	B3GNT5

Retention of Extracellular Matrix Proteins in the resulting Decellularized Scaffold

The purpose of decellularization was to remove cellular content while preserving the structural proteins of the extracellular matrix. Nine noncollagenous extracellular matrix proteins were analyzed by mass spectrometry before and after decellularization. Of these, FMOD, DAG1, FBN1, ACAN, and DCN were depleted to levels below the limit of detection. Noncollagenous ECM proteins were partially retained in the

decellularized scaffold and may contribute to the successful recellularization process. These include MFGE8, HAPLN1, TNC, and BGN. Noncollagenous proteins and their extent of depletion are shown in table 9.

Table 9 Extracellular matrix noncollagenous proteins depleted by decellularization process

Extracellular matrix noncollagenous proteins	% depleted	Gene symbol
Fibromodulin	100	FMOD
Dystroglycan	100	DAG1
Fibrillin-1	100	FBN1
Aggrecan core protein	100	ACAN
Decorin	100	DCN
Lactadherin	98	MFGE8
Hyaluronan and proteoglycan link protein 1	90	HAPLN1
Tenascin	70	TNC
Biglycan	57	BGN

39 collagen alpha chains were analyzed before and after decellularization to assess collagenous composition of the resulting decellularized scaffold. The collagen alpha chains were detected in native cartilage by mass spectrometry. After the decellularization process, nine of these were no longer detectable. Blue bars show composition of cartilage before the decellularization process, and red bars show composition of the scaffold after the decellularization process. The resulting decellularized scaffold comprised predominantly of COL2A1, COL1A1, COL6A1, COL1A2, COL11A1, COL11A2, COL3A1, COL5A1, COL5A2, COL5A3, COL4A5,

COL4A2, and COL4A3. Minor contributions of COL7A1, COL16A1, COL22A1, COL27A1, COL28A1, COL12A1, COL13A1, COL14A1, and COL17A1 were detected after decellularization, as shown in figure 10.

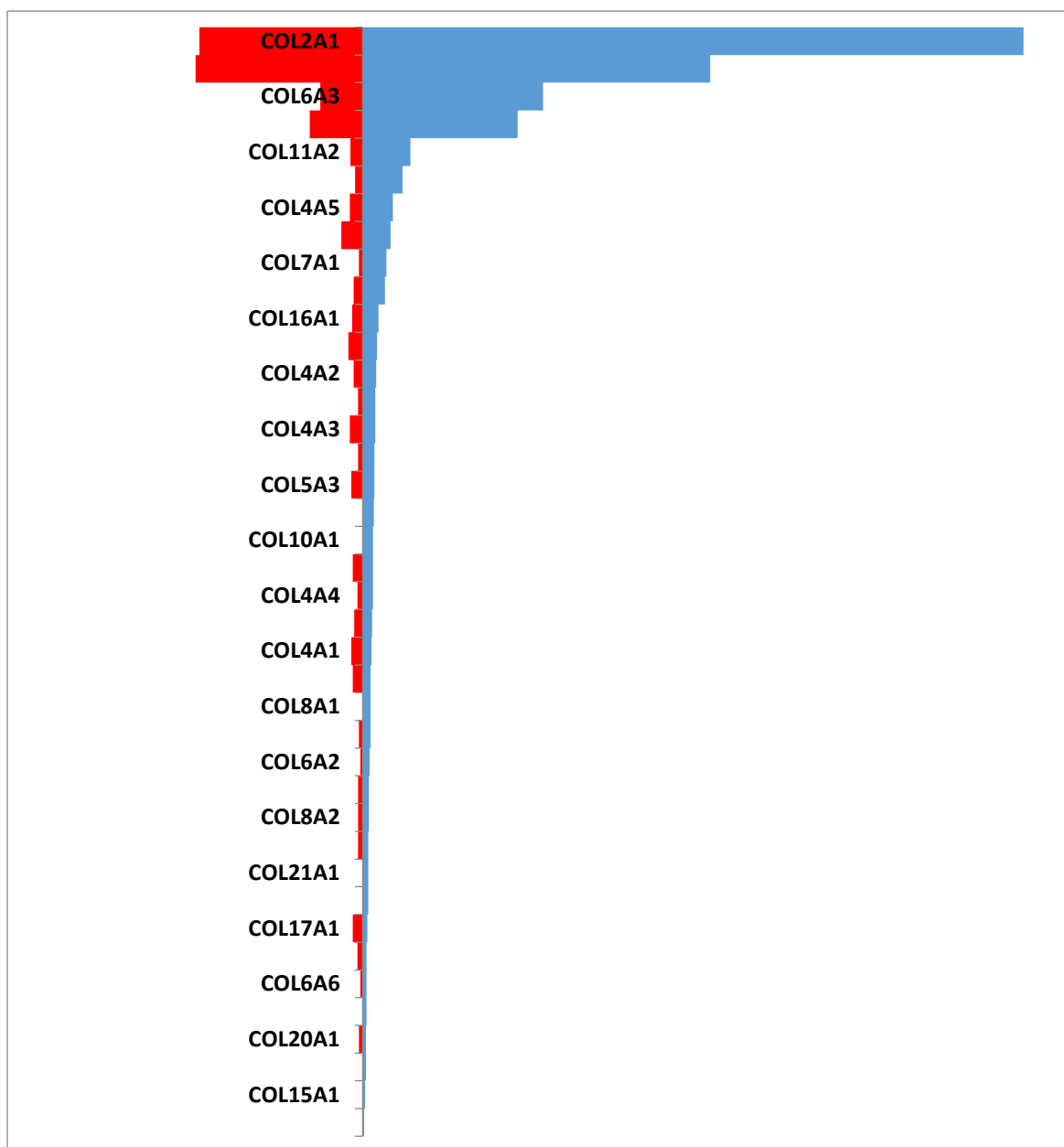


Figure 10 Composition of cartilage before (blue) and after (red) decellularization

Future work should aim to better understand each of these proteins functions and how it relates to cartilage.

Histology

In order to visualize the microscopic anatomy of cells and tissues, histology was used. figure 11 shows the non-decellularized porcine cartilage before processing with an H&E Stain.

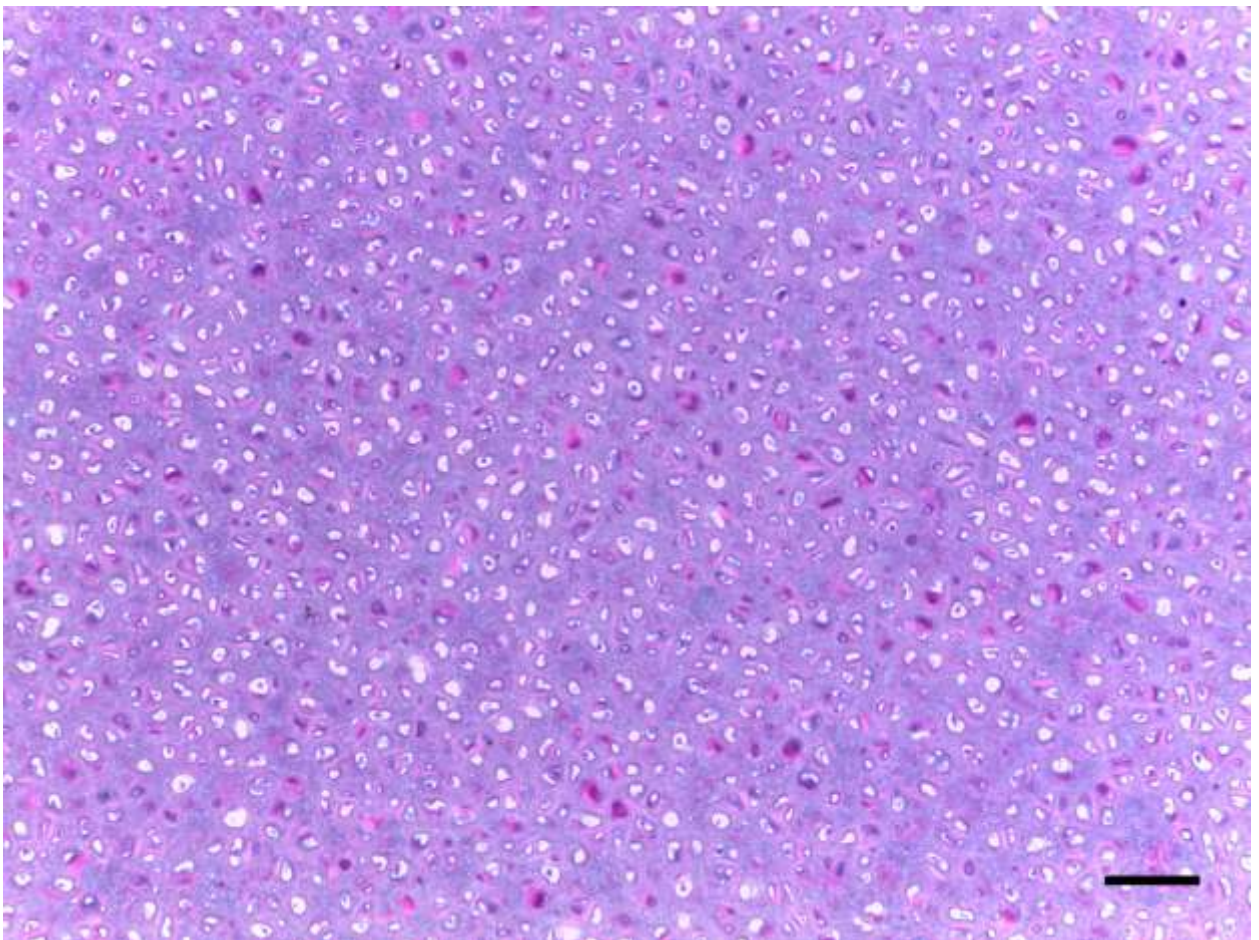


Figure 11 H&E Stain on Non-Decellularized Cartilage. 10x Transverse Image, with a scale bar of 100 μ m

Figure 12 shows the final decellularized H&E stain.

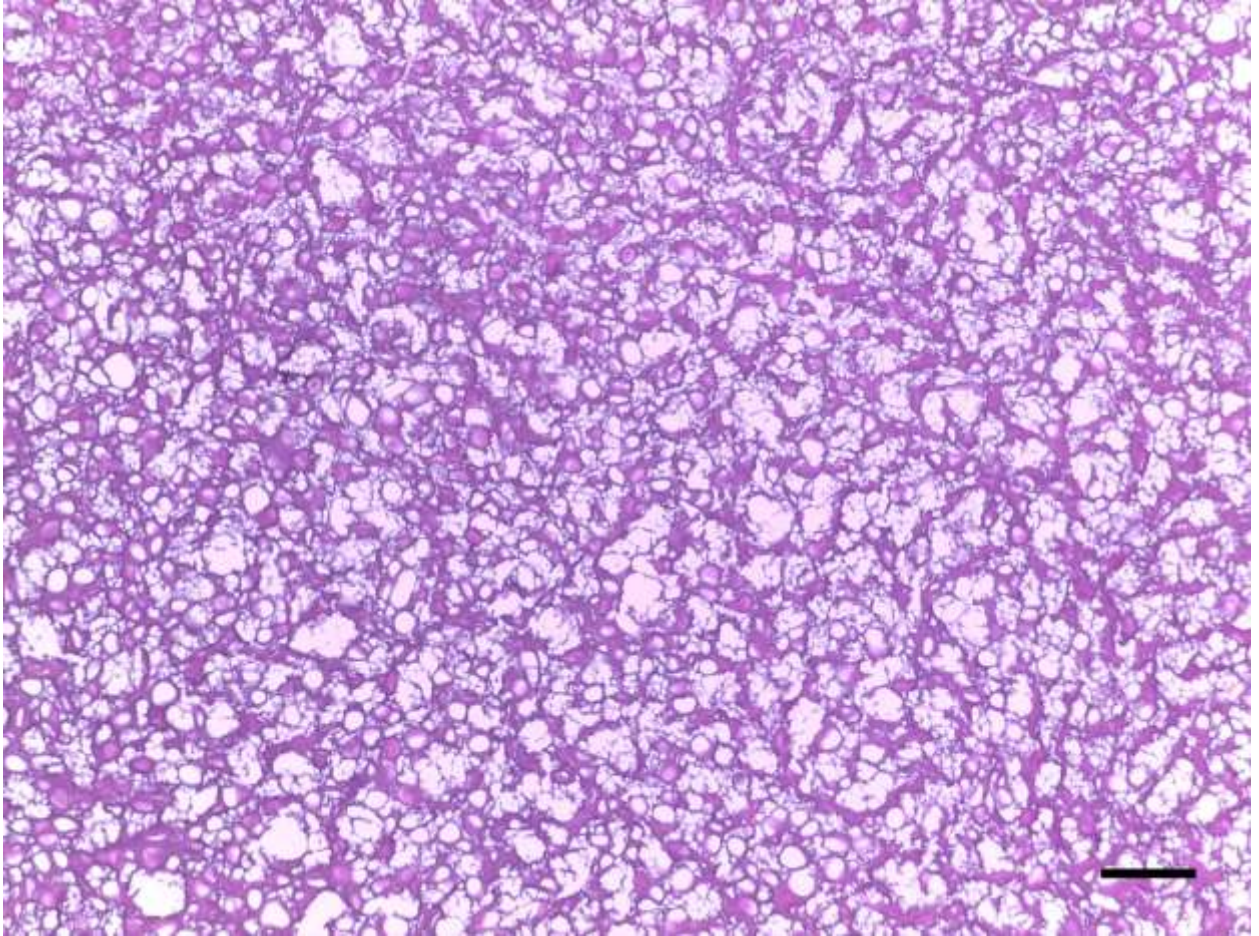


Figure 12 H&E Stain on Final Decellularized Cartilage. 10x Transverse Image, with a scale bar of 100 μ m

Figure 13 shows the final decellularized Alcian Blue stain. Alcian Blue stain was not noticeably detectable in the non-decellularized cartilage.

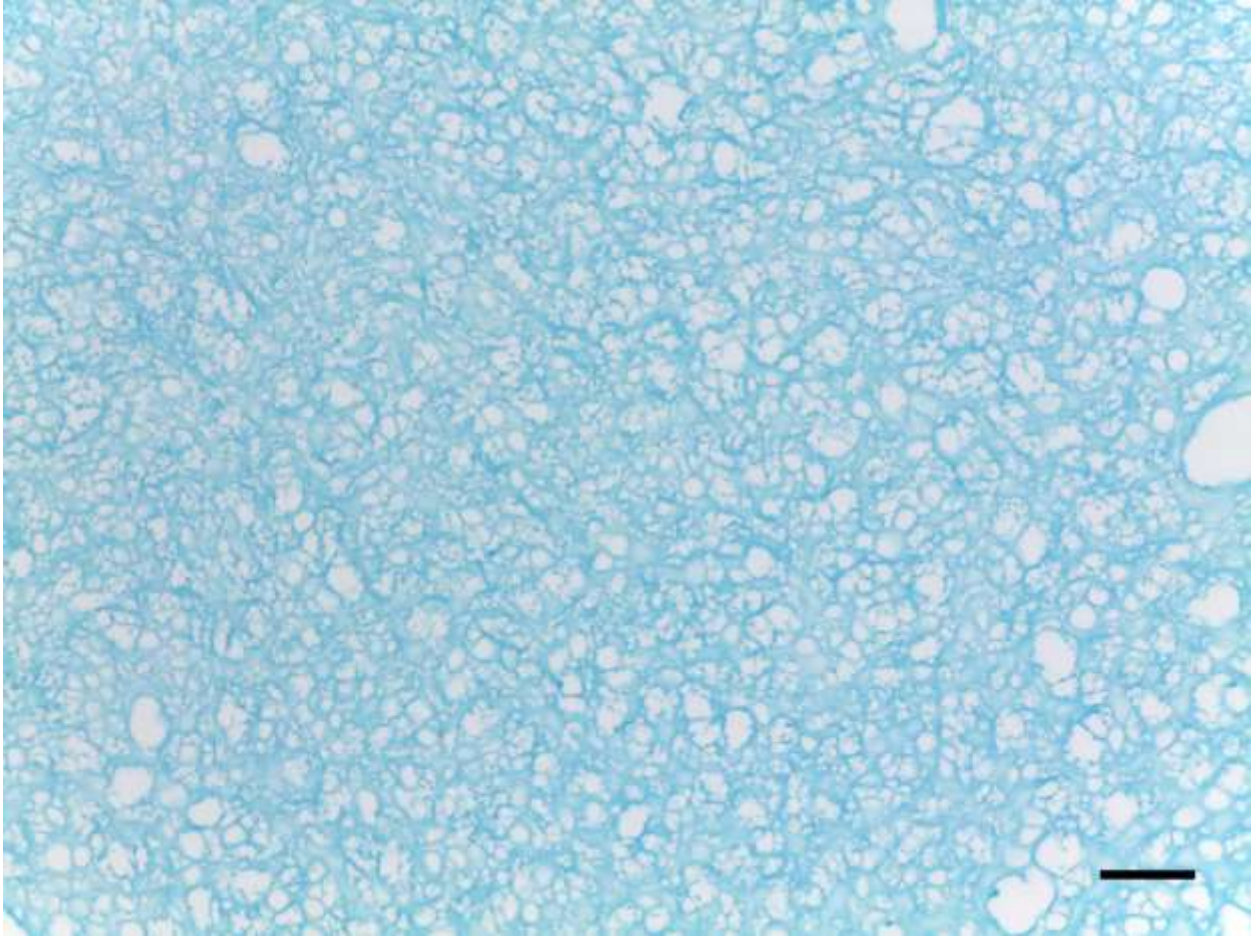


Figure 13 Alcian Blue Stain on Final Decellularized Cartilage. 10x Transverse Image, with a scale bar of 100 μm

Histological analysis showed a decrease in cellular structures, with the preservation of the extracellular collagen fiber networks.

Hoechst Evaluation

Hoechst stain is specific for DNA and results in a blue stain. The samples were imaged on a Zeiss Confocal LSM 510 Meta microscope. The Hoechst stain images, as shown in figure 14, confirmed that DNA was removed as a result of the decellularization wash cycles.

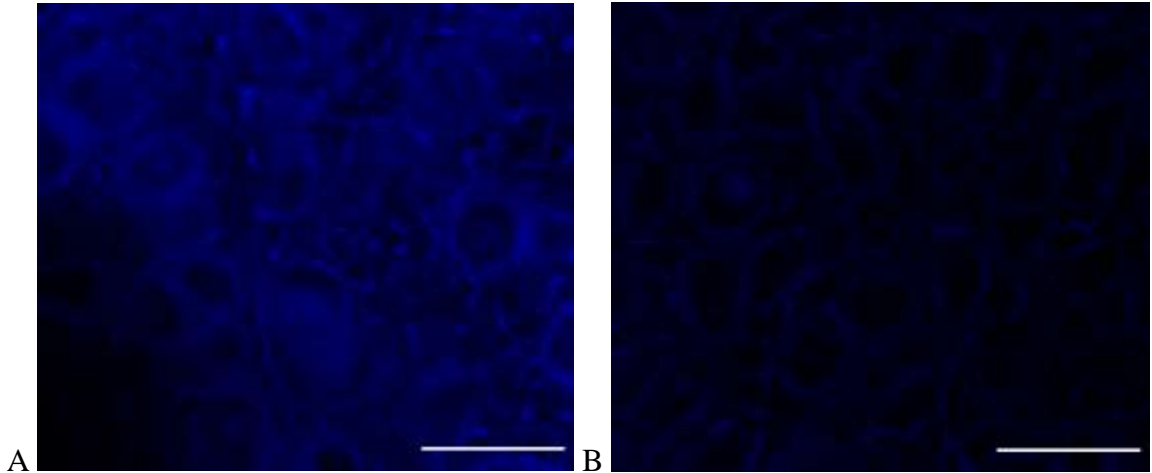


Figure 14 Hoechst Stain at 40x, with a scale bar of 50 μm . A) Non-Decellularized Sample. B) Decellularized Sample

SEM Preparation and Imaging

SEM confirmed that the decellularization wash cycles successfully resulted in making the scaffold more porous. The collagen fibers of the ECM were isolated during the process. The surface of a non-decellularized cartilage disc is shown in figure 15 with a scale bar of 20 μm .



Figure 15 Non-Decellularized Cartilage Disk. Scale bar of 20 μ m

Figure 16 shows the final decellularized cartilage discs surface with a scale bar of 20 μ m.

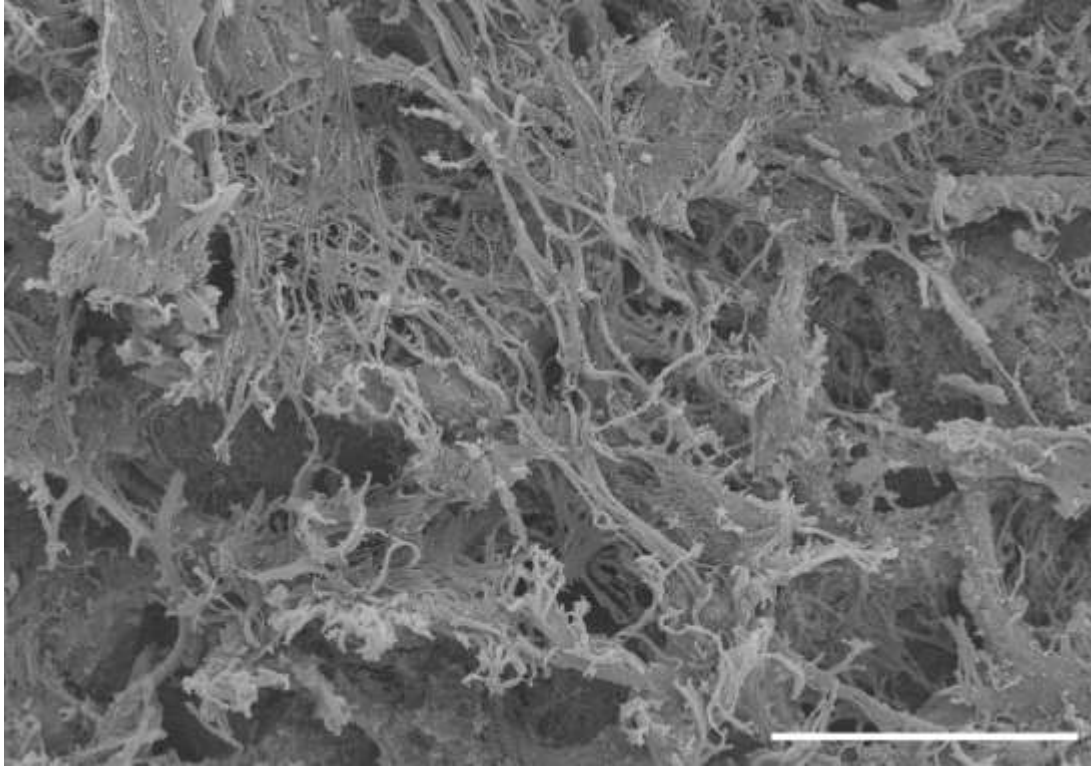


Figure 16 Final Decellularized Cartilage Disk. Scale bar of 20 μ m

Characterization After Recellularization

Histology

Samples were processed the same way as described for the non-decellularized and decellularized samples. The cellular samples were imaged at weeks one, two, and three after seeding with C28/I2 cells. The Boise State B scaffolds were imaged at the end of their eight-month incubation period. Figure 17 shows the recellularized Boise State B Cartilage Sample with C28/I2 cells in both the Alcian Blue Stain and H&E Stain.

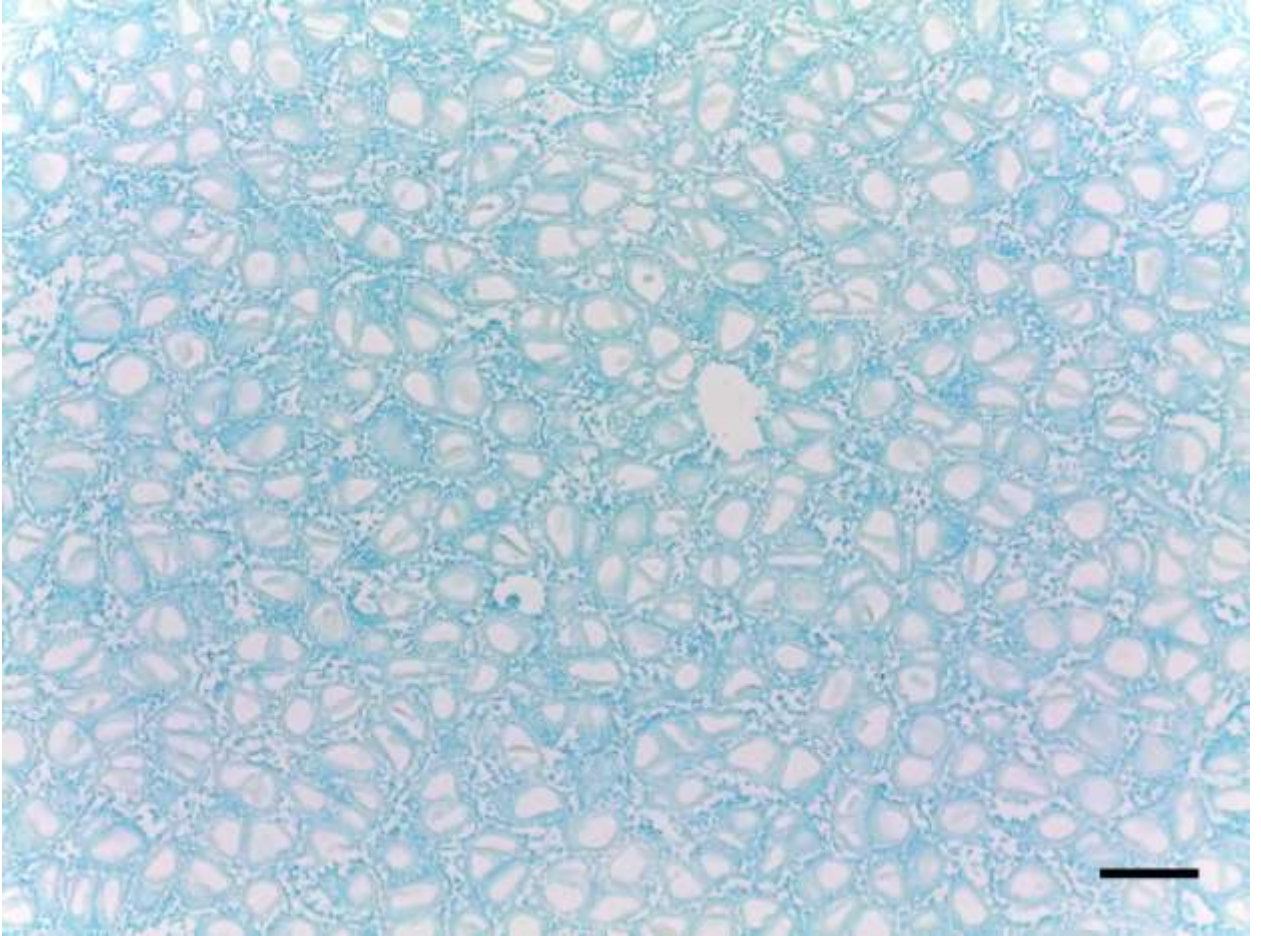


Figure 17 Recellularized Boise State B Cartilage Sample with Alcian Blue Stain at 20x, with a scale bar of 50 μm

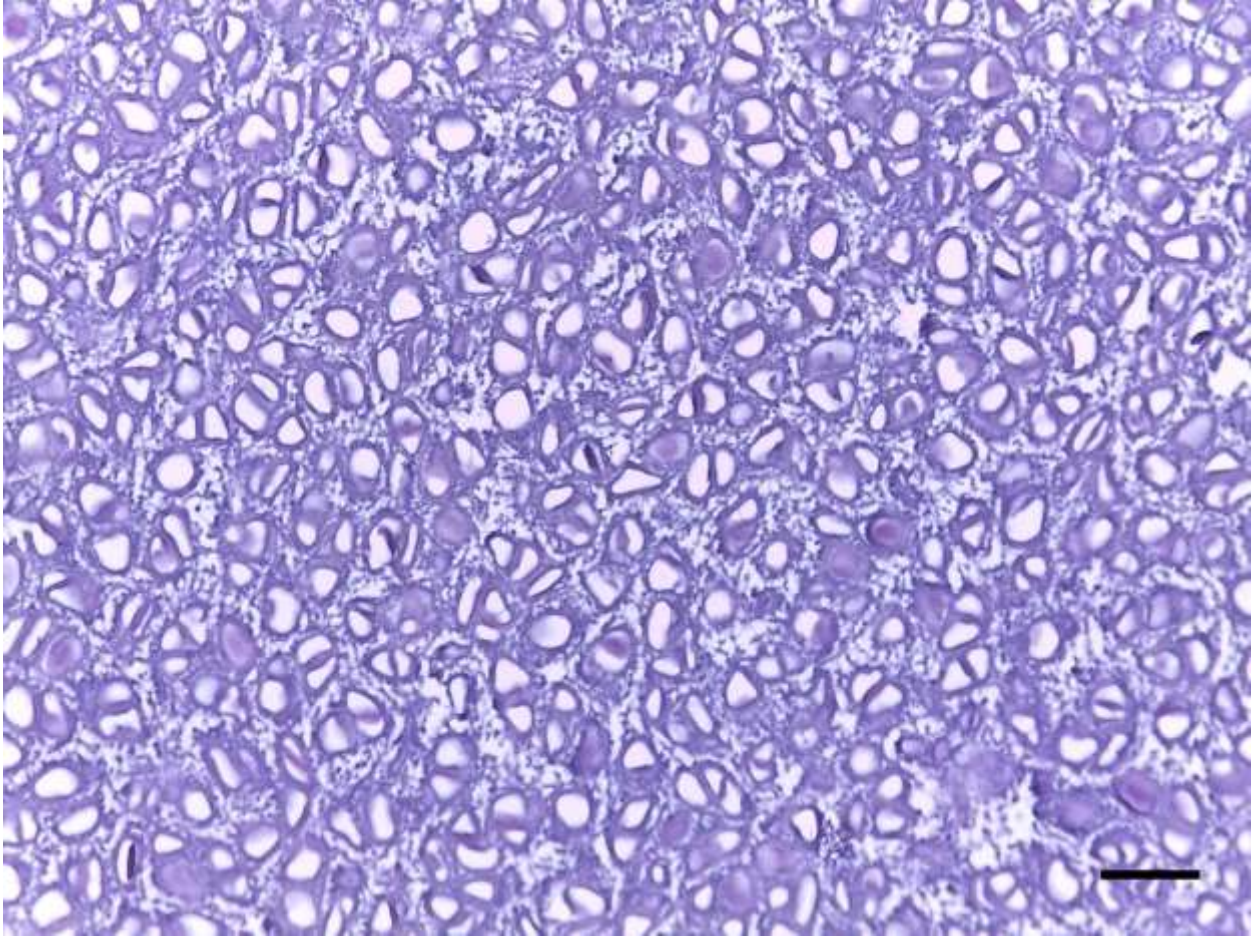


Figure 18 Recellularized Boise State B Cartilage Sample with H&E Stain at 20x, with a scale bar of 50 μm

SEM Imaging

Samples were processed the same way as described for the non-decellularized and decellularized samples. The cellular samples were imaged at weeks one, two, and three after seeding with the C28/I2 cells. The Boise State *B* scaffolds were imaged at the end of their eight-month incubation period. Figure 19 shows cells adhering to the cellular scaffold in week one.

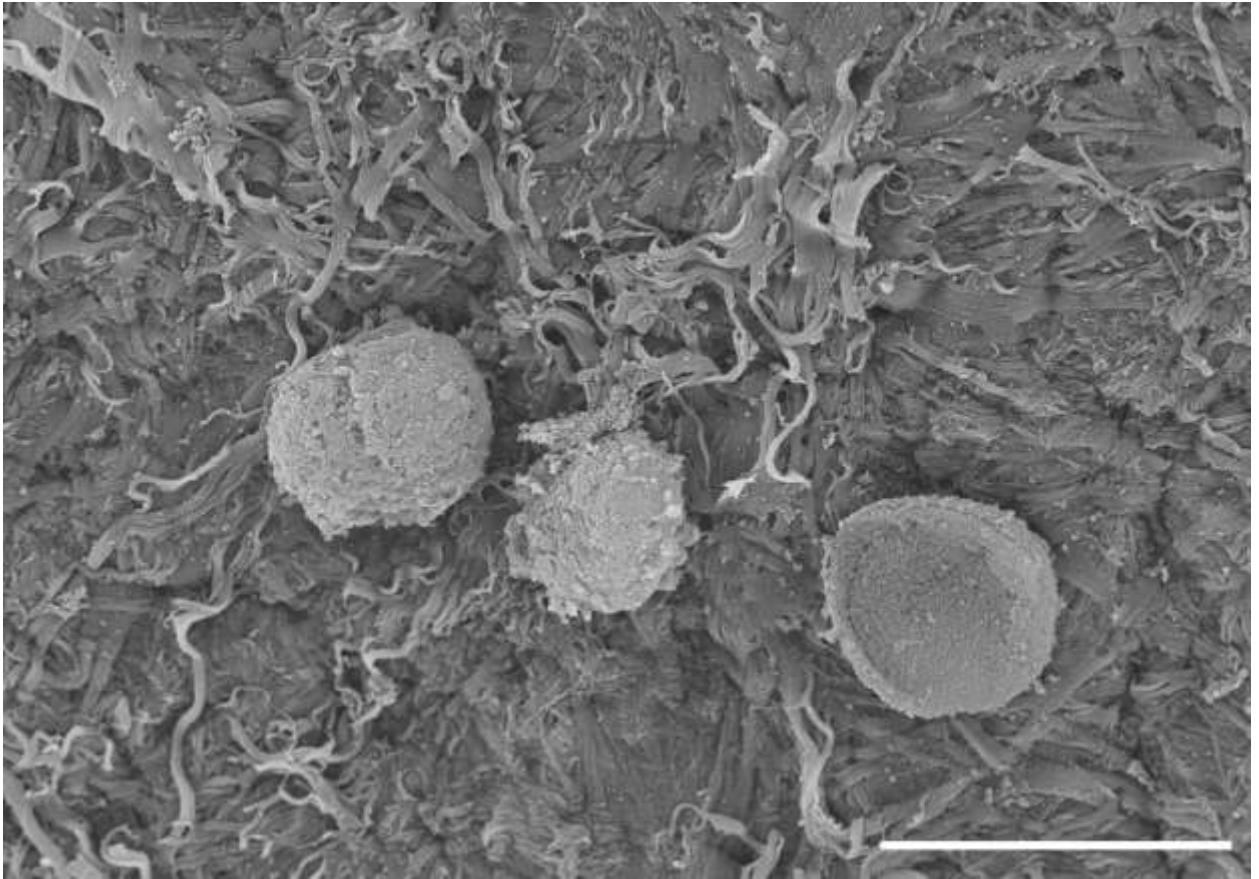


Figure 19 Recellularized Cartilage Disk with C28/I2 Cells at week 1. Scale bar of 20 μ m

Figure 20 shows bundles of cells on the recellularized Boise State *B* scaffolds at the eight-month time point.

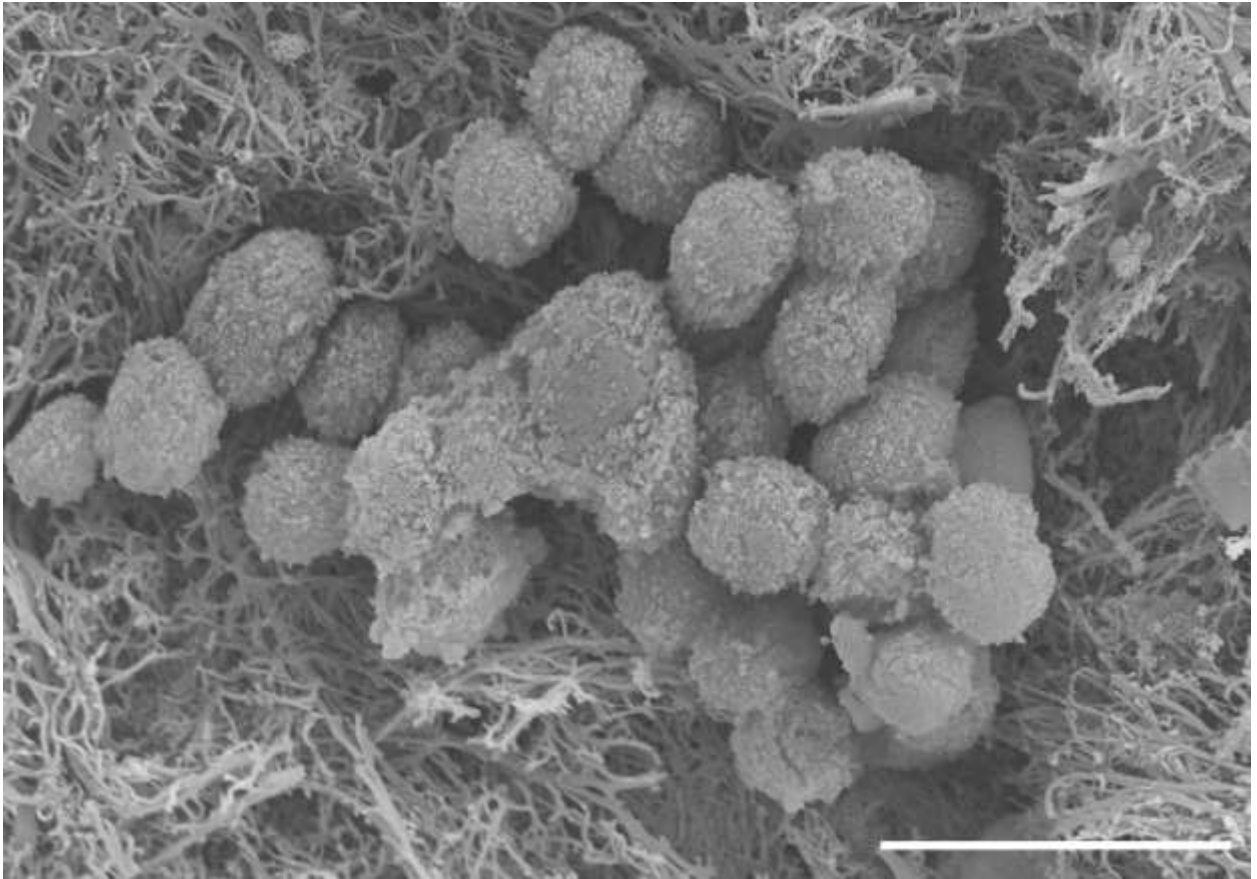


Figure 20 Recellularized Boise State B shaped Cartilage Disk with C28/I2 Cells at 8 months. Scale bar of 20 μ m

These SEM images showed that overtime the cells did proliferate on the surface of the scaffold. They formed clusters of cells in various places among the collagen fibers in comparison to individual cells, as shown in week one images. There was very little change in comparison of week one, two, and three time points.

Characterization of Cellular Response to the Scaffolds

In order to understand the cellular response during recellularization, a molecular biology approach was used. Real-time quantitative PCR was used. As a control, cells were also grown on tissue culture (TC) plastic under standard culture conditions to

evaluate cellular responses and to determine if the decellularized scaffold helps influence chondrogenesis.

Q-RT-PCR

Selection of housekeeping genes

Five candidate housekeeping genes, as listed in table 10, were compared for all experimental conditions used in this study to identify those that remain constant and, therefore, may serve as appropriate housekeeping genes controls. GAPDH and HPRT were selected as the housekeeping gene for normalization in these experiments based on comparison to three other candidate housekeeping genes; both were found to be stably expressed independently of experimental conditions based on minimum variance. Correlation analysis confirmed that GAPDH and HPRT expression levels are correlated throughout the experiments, as demonstrated in figure 21.

Table 10 Housekeeping genes

	ACTB					
		87.4				
	B2M	9				
DH	GAP	140.54	10.77			
1	HPRT	135.44	9.01	✓ 0.11		
0	RPLP	125.96	7.34	1.49	0.91	
	ACTB	M	B2	DH	T1	P0
			GAP		HPR	RPL

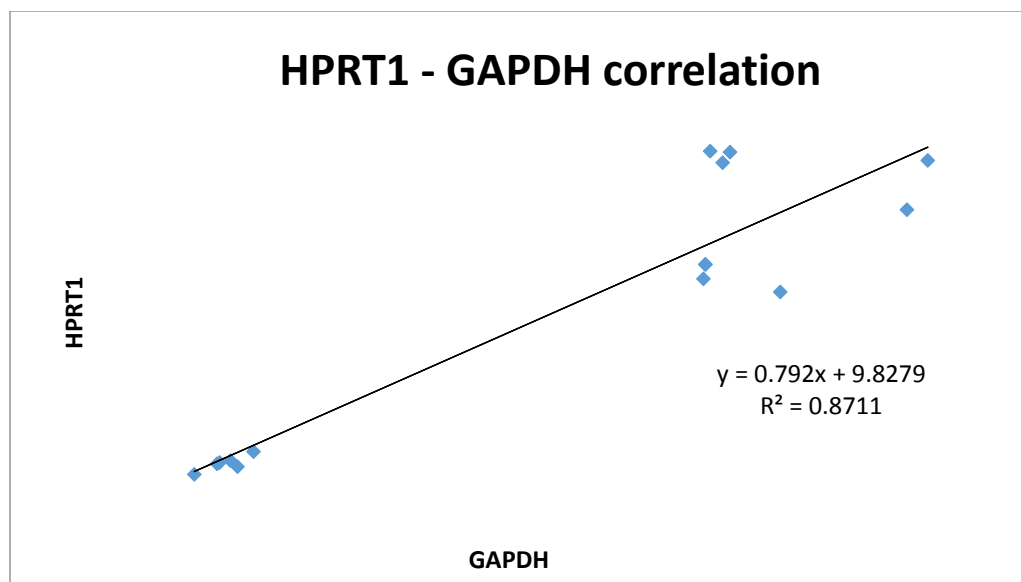


Figure 21 HPRT1 - GAPDH correlation

Comparison of Scaffold versus Plastic

Relative abundance of genes associated with chondrogenesis was calculated and reported here as mean plus/minus standard deviation. As shown in figure 22, gene expression is induced under control chondrogenic conditions on tissue culture plastic, indicated by data points above the diagonal line (figure 22). In figure 23, the diagonal line indicates the trend expected if there is no difference between the cellular response when cells are grown on the cartilage scaffold versus grown on tissue culture plastic. Data points above the line reflect genes expressed at higher levels on the cartilage scaffold compared to plastic. Data points below the line indicate genes that are expressed at higher levels on plastic compared to the cartilage scaffold. Data points that fall on the line were not changed (figure 23).

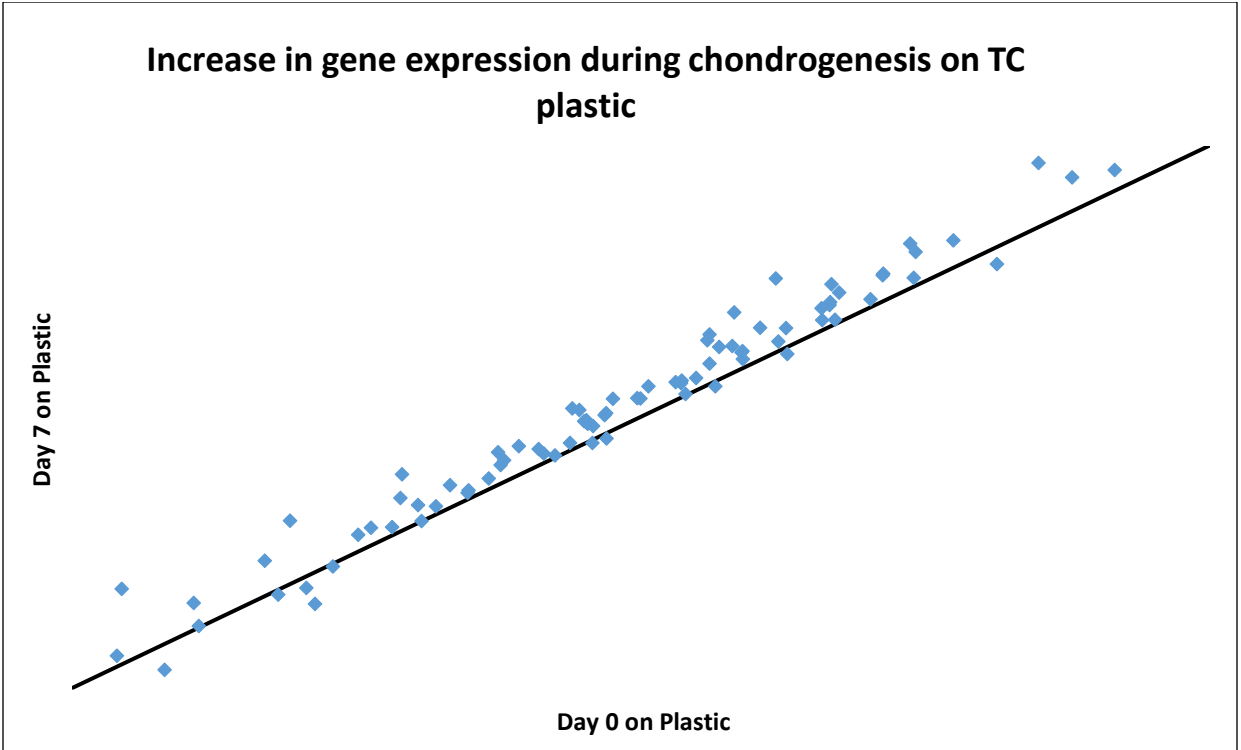


Figure 22 Increase in gene expression during chondrogenesis on TC plastic

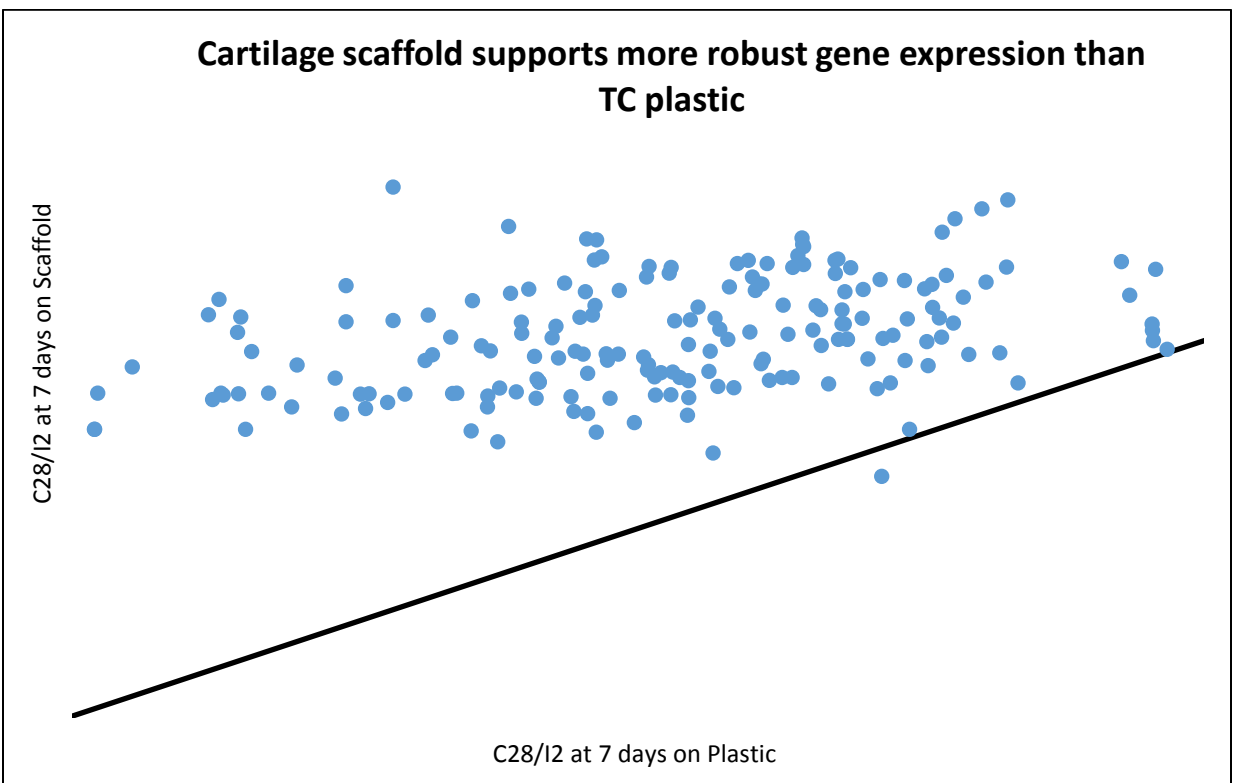


Figure 23 Cartilage scaffold supports more robust gene expression than TC plastic

A total of 76 genes were analyzed during chondrocyte differentiation for seven days. A total of 52 genes were upregulated during seven days of chondrocyte differentiation on standard TC plastic (figure 22). Of those 52 genes, 33 genes in cells cultured on decellularized 3-D (three-dimensional) porcine scaffold showed an increase in expression. A total of 19 genes were upregulated on tissue culture plastic during chondrogenesis; but, were not upregulated significantly during the same period by cells cultured on decellularized porcine cartilage scaffold. A total of 25 genes were upregulated during chondrogenesis on the cartilage scaffold that was not observed to be upregulated on tissue culture plastic under standard 2-D (two-dimensional) culture conditions (figure 23).

Of the genes unique to the scaffold not seen on TC plastic, the protein functions were investigated and summarized in table 11.

Table 11 Chondrogenic markers expressed by chondrocytes that are enhanced by growth on the scaffold not seen on TC plastic and their function

Genes Unique to Scaffold not seen on TC Plastic			
Gene symbol	Name	Function	Reference
CDH1	Cadherin-1	Provides instruction for making a protein called epithelial cadherin, which is found in the membrane that surrounds epithelial cells. This family of proteins functions to help neighboring cells stick together to form organized tissues. Cell Adhesion.	(Tomschy, Fauser, Landwehr, & Engel, 1996)
CLEC3B	C-type lectin domain family 3, member B	Encodes for a protein called Tetranectin. Cellular response to transforming growth factor stimulus.	(Mazzoni et al., n.d., 2019)
COL12A1	Collagen, type XII, alpha 1	Encodes for the alpha chain of type XII collagen. Modifies the interactions between Collagen fibrils and the surrounding matrix. A component of Cartilage ECM.	(Agarwal et al., 2012)
COL15A1	Collagen, type XV, alpha 1	Encodes the alpha chain of type XV collagen. Strongest expression in basement membrane zones may function to adhere basement membranes to underlying connective tissue.	(Karlsson et al., 2010)
CTGF	Connective tissue growth factor	Modulates signaling pathways leading to cell adhesion and migration, along with ECM deposition and remodeling, which together lead to tissue remodeling.	(Lipson, Wong, Teng, & Spong, 2012)
CTNND1	Catenin (cadherin-associated protein), delta 1	Functions in adhesion between cells and signal transduction. Helps regulate the maintenance of the superficial zone of Articular cartilage.	(Taniguchi et al., 2009)

ECM1	Extracellular matrix protein 1	Inhibits chondrocyte hypertrophy, matrix mineralization, and endochondral bone formation.	(Kong et al., 2010)
ICAM1	Intercellular adhesion molecule 1	Encodes a cell surface glycoprotein, which is typically expressed on endothelial cells and cells of the immune system. On the surface of osteoblasts, and might also be involved in the regulation of joint diseases.	(Rangkasenee et al., 2020)
ITGA3	Integrin, alpha 3 (antigen CD49C, alpha 3 subunit of VLA-3 receptor)	Involved in cell adhesion and collagen binding.	(Zhang & Zhang, 2019)
ITGA4	Integrin, alpha 4 (antigen CD49D, alpha 4 subunit of VLA-4 receptor)	Functions in cell surface adhesion and signaling, ECM receptor interaction.	(Zhu et al., 2017)
ITGA6	Integrin, alpha 6	Functions in cell surface adhesion and signaling.	(Lapointe, Verpoorte, & Stevens, 2013; Tu et al., 2020)
ITGAM	Integrin, alpha M (complement component 3 receptor 3 subunit)	Cell adhesion-related molecules.	(Wang et al., 2019)
ITGB3	Integrin, beta 3 (platelet glycoprotein IIIa, antigen CD61)	Participates in cell adhesion as well as cell surface-mediated signaling.	(Fabiana N. Soki, Ryu Yoshida, 2018)
ITGB5	Integrin, beta 5	Cell surface receptors that participate in cell adhesion as well as cell surface-mediated signaling. Remodeling component for articular cartilage.	(Adapala & Kim, 2016)

KAL1 (Anos1)	Anosmin 1	Found in zones of articular cartilage ECM, Cell Surface Protein.	(Grogan et al., 2014)
LAMA1	Laminin, alpha 1	Major component of the basement membrane. Associated with cell adhesion, differentiation, migration, and signaling.	(Mann et al., 2019)
MMP10	Matrix metalloproteinase 10 (stromelysin 2)	Involved in the breakdown of extracellular matrix in normal physiological processes, such as tissue remodeling.	(Proteomics, Of, To, & Injury, 2018)
MMP12	Matrix metalloproteinase 12	Involved in the breakdown of extracellular matrix in normal physiological processes, such as tissue remodeling.	(Lv et al., 2016)
MMP9	Matrix metalloproteinase 9 (gelatinase B, 92kDa gelatinase, 92kDa type IV collagenase)	Involved in the breakdown of extracellular matrix in normal physiological processes, such as tissue remodeling.	(Miao et al., 2004)
SELP	Selectin P (granule membrane protein 140kDa, antigen CD62)	This protein redistributes to the plasma membrane during platelet activation and degranulation.	(Gari et al., 2016)
SGCE	Sarcoglycan, epsilon	Links the actin cytoskeleton to the ECM.	(Rouillard et al., 2016)
SPG7	Spastic paraplegia 7 (pure and complicated autosomal recessive)	Roles in diverse cellular processes including membrane trafficking, intracellular motility, organelle biogenesis, protein folding, and proteolysis.	(Bonn, Pantakani, Shoukier, Langer, & Mannan, 2010)
THBS3	Thrombospondin 3	Mediates cell-to-cell and cell-to-matrix interactions. Found in developing cartilage.	(Hankenson, Hormuzdi, Meganck, &

			Bornstein, 2005)
VCAN	Versican	Major component of the ECM; involved in cell adhesion and proliferation during chondrogenesis.	(Sztrolovics et al., 2002)
VTN	Vitronectin	ECM markers that promote cell adhesion and spreading.	(Vieira et al., 2015)

Markers of Chondrogenesis detected by Mass Spectrometry after growth on Decellularized Scaffold

Figure 24 summarizes the results of proteomic analysis after recellularization of the decellularized scaffold.

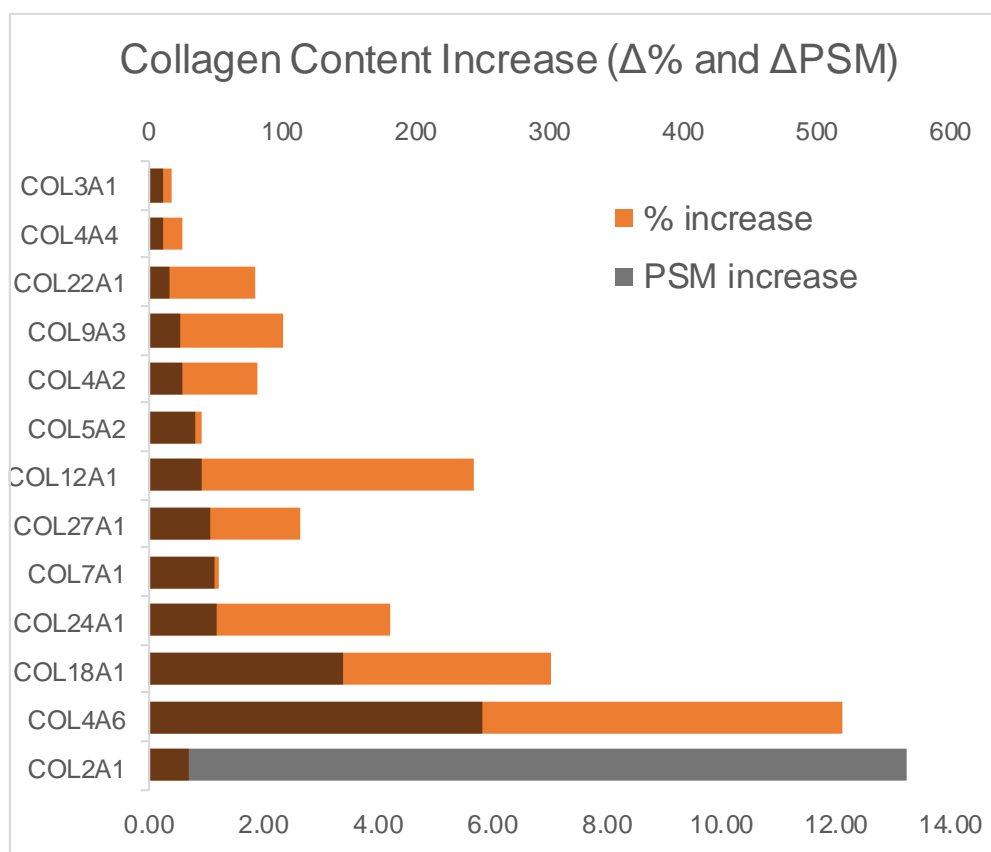


Figure 24 Percent Change of Collagen Content

CHAPTER SIX: CONCLUSIONS AND FUTURE WORK

To our knowledge, this study represents the first demonstration of biomarkers for decellularization of a Porcine ear for cartilage regeneration. After dissecting a Porcine ear to isolate the cartilage, a series of four wash cycles took place to remove unwanted cellular materials. The Sodium Acetate and Guanidine Hydrochloride wash were to denature and remove noncollagenous components. The SDS, Tris, HCL, EDTA, MgCl₂, DTT, and Triton-X wash were to decrease ECM proteins, alter the microstructure of collagen fibers, and cause agglutination of DNA. The Hyaluronidase wash was to remove HA and proteoglycan inside the cartilage disk. The DNase and RNase wash were to break down DNA and RNA, followed by a freeze-thaw cycle to increase porosity. Freeze-thaw cycles in between wash cycles were to increase porosity and kill innate chondrocytes.

Data compiled includes results from DNA extraction, a Hoechst evaluation, Histology, SEM, Mass spectrometry, and PCR. It was concluded that the decellularization wash cycles successfully resulted in decellularizing the porcine cartilage scaffold. Traditionally, laboratories have monitored DNA content to determine if cells have been removed since all cells contain DNA. However, there may be false-positive signals for DNA that does not indicate that cells are still present. Therefore, additional components were analyzed of cells, and mass spectrometry was used to measure the removal of cellular components including nuclei, mitochondria, cytosol, rough endoplasmic reticulum, plasma membrane, and Golgi. These additional measures showed that the cells were removed below the threshold of detection.

A more aggressive decellularization wash cycle could have been used in the beginning to avoid repeating wash cycles. Future work could be done to monitor component changes at each level of decellularization. At the end of decellularization in this experiment, a 92 % decrease was observed between the non-decellularized material and the final decellularized material. The 8% of material left behind is thought to be because of the biochemistry within the ECM. These remaining materials could be “sticky,”; therefore, the proteins are determined not fully depleted after decellularization and would not qualify as sufficient markers. Previous work has not fully analyzed what is left behind after decellularization. Future work should be done to better understand the material left behind after decellularization as it is important when evaluating laboratory-generated cartilage for patient-specific biocompatibility.

The scaffold was shown to be more porous after decellularization in both SEM and Histology when compared to its original material. Visual cell components present in the non-decellularized histology images were not shown in the decellularized images. No cells were shown to be present in histology images after the decellularized scaffolds were recellularized. Future work could be done using a binding protein to increase cell proliferation inside the scaffold. Future work could also consider looking at if cells are needed inside the scaffold. Mechanical testing was not done in this experiment but should be done to understand the strength of these cartilage disks in comparison to healthy human cartilage.

It is not recommended to do media changes so early in cell culture. Adding fresh media only, could prevent cells loosely adhered to the surface of the scaffold from being lost during incubation periods. SEM images showed cells could attach and proliferate on

the surface of the scaffold. The cells also express genes, as shown in PCR and Proteomic data.

The collagen fibers of the ECM were isolated during the process. To characterize the scaffold remaining after decellularization, collagens present by mass spectrometry were analyzed. Thirty-nine collagen alpha chains were detected in native cartilage by mass spectrometry. After the decellularization process, nine of these were no longer detectable.

This study is novel because it looks at new knowledge by analyzing proteins that make up the decellularized porcine tissue and the recellularized scaffold. It provides insight on acceptable markers for decellularization by looking at a profile of markers instead of just one or two proteins. The use of other cell lines could benefit this field of research by using patient-specific MSC's or pre-chondrocytes. A major limitation of this study was also that it mainly looked at short term changes. The scaffolds grown up to eight months showed an increase in cellular adhesion and proliferation. Future experiments in cell culture should be longer in duration.

Overall, this novel research shows promise that laboratory-generated cartilage could be a future alternative treatment option for individuals suffering from OA. These cartilage discs can be made to fit any cartilage lesion. This approach aims to restore the patient's natural anatomy and prevent the need of a joint replacement. Using decellularization to create biomaterials can generate biocompatible scaffolds. Patient-specific chondrocytes can promote differentiation that in the long term is predicted to lead to healing damaged tissue.

REFERENCES

- Adapala, N. S., & Kim, H. K. W. (2016). *Comprehensive Genome-Wide Transcriptomic Analysis of Immature Articular Cartilage following Ischemic Osteonecrosis of the Femoral Head in Piglets*. 1–17. <https://doi.org/10.1371/journal.pone.0153174>
- Agarwal, P., Zwolanek, D., Keene, D. R., Schulz, J., Blumbach, K., Heinegård, D., ... Eckes, B. (2012). *Collagen XII and XIV , New Partners of Cartilage Oligomeric Matrix Protein in the Skin Extracellular Matrix*. 287(27), 22549–22559. <https://doi.org/10.1074/jbc.M111.335935>
- Bonn, F., Pantakani, K., Shoukier, M., Langer, T., & Mannan, A. U. (2010). *Functional Evaluation of Paraplegin Mutations by a Yeast Complementation Assay*. <https://doi.org/10.1002/humu.21226>
- Cheng, C. W., Solorio, L. D., & Alsberg, E. (2014). Decellularized tissue and cell-derived extracellular matrices as scaffolds for orthopaedic tissue engineering. *Biotechnology Advances*, 32(2), 462–484. <https://doi.org/10.1016/j.biotechadv.2013.12.012>
- Chomczynski P, S. N. (1987). Single-step method of RNA isolation by acid guanidinium thiocyanate-phenol-chloroform extraction. *Anal Biochem*, 162(1), 156- 159. <https://doi.org/10.1006/abio.1987.9999>
- Cross, M., Smith, E., Hoy, D., Nolte, S., Ackerman, I., Fransen, M., ... March, L. (2014). The global burden of hip and knee osteoarthritis: Estimates from the Global Burden of Disease 2010 study. *Annals of the Rheumatic Diseases*, 73(7), 1323–1330. <https://doi.org/10.1136/annrheumdis-2013-204763>
- Djouad, F., Mrugala, D., Noël, D., & Jorgensen, C. (2006). Engineered mesenchymal stem cells for cartilage repair. *Regenerative Medicine*, 1(4), 529–537. <https://doi.org/10.2217/17460751.1.4.529>

- Elder, B. D., Eleswarapu, S. V., & Athanasiou, K. A. (2009). Biomaterials Extraction techniques for the decellularization of tissue engineered articular cartilage constructs. *Biomaterials*, *30*(22), 3749–3756.
<https://doi.org/10.1016/j.biomaterials.2009.03.050>
- Escobar Ivirico, J. L., Bhattacharjee, M., Kuyinu, E., Nair, L. S., & Laurencin, C. T. (2017). Regenerative Engineering for Knee Osteoarthritis Treatment: Biomaterials and Cell-Based Technologies. *Engineering*, *3*(1), 16–27.
<https://doi.org/10.1016/J.ENG.2017.01.003>
- Fabiana N. Soki, Ryu Yoshida, D. N. P. (2018). Articular cartilage protection in Ctsk -/- mice is associated with cellular and molecular changes in subchondral bone and cartilage matrix. *Center for Molecular Medicine*, 8666–8676.
<https://doi.org/10.1002/jcp.26745>
- Fan, H., & Gulley, M. L. (n.d.). *DNA Extraction from Fresh or Frozen Tissues*. *49*, 5–11.
- Gari, M. A., Alkaff, M., Alsehli, H. S., Dallol, A., Gari, A., Abu-elmagd, M., ... Abbas, M. M. (2016). Identification of novel genetic variations affecting osteoarthritis patients. *BMC Medical Genetics*, *17*(Suppl 1), 0–4.
<https://doi.org/10.1186/s12881-016-0330-2>
- Gilpin, A., & Yang, Y. (2017). Decellularization Strategies for Regenerative Medicine: From Processing Techniques to Applications. *BioMed Research International*, *2017*. <https://doi.org/10.1155/2017/9831534>
- Goldberg, A., Mitchell, K., Soans, J., Kim, L., & Zaidi, R. (2017). The use of mesenchymal stem cells for cartilage repair and regeneration: A systematic review. *Journal of Orthopaedic Surgery and Research*, *12*(1), 1–30.
<https://doi.org/10.1186/s13018-017-0534-y>
- Gong, Y. Y., Xue, J. X., Zhang, W. J., Zhou, G. D., Liu, W., & Cao, Y. (2011). A sandwich model for engineering cartilage with acellular cartilage sheets and chondrocytes. *Biomaterials*, *32*(9), 2265–2273.
<https://doi.org/10.1016/j.biomaterials.2010.11.078>
- Grogan, S. P., Duffy, S. F., Pauli, C., Koziol, J. A., Su, A. I., Lima, D. D. D., & Lotz, M.

- K. (2014). *NIH Public Access*. 65(2), 418–428.
<https://doi.org/10.1002/art.37760>.Zone-specific
- Gupta PK et al. (2012). *Mesenchymal stem cells for cartilage repair in osteoarthritis*.
<https://doi.org/10.1186/scrt116>
- Hankenson, K. D., Hormuzdi, S. G., Meganck, J. A., & Bornstein, P. (2005). *Mice with a Disruption of the Thrombospondin 3 Gene Differ in Geometric and Biomechanical Properties of Bone and Have Accelerated Development of the Femoral Head*. 25(13), 5599–5606. <https://doi.org/10.1128/MCB.25.13.5599>
- Heath, D. E. (2019). *A Review of Decellularized Extracellular Matrix Biomaterials for Regenerative Engineering Applications signed to work with biology to improve the regenerative*. 155–166.
- Helmick, C. G., Felson, D. T., Lawrence, R. C., Gabriel, S., Hirsch, R., Kwoh, C. K., ... Stone, J. H. (2008). Estimates of the prevalence of arthritis and other rheumatic conditions in the United States. Part I. *Arthritis and Rheumatism*, 58(1), 15–25.
<https://doi.org/10.1002/art.23177>
- Hsueh, M., Khabut, A., Kraus, B., Biology, M. S., & Biology, S. (2017). *HHS Public Access*. 15(2), 374–388.
<https://doi.org/10.1021/acs.jproteome.5b00946>.Elucidating
- Karlsson, C., Dehne, T., Lindahl, A., Brittberg, M., Pruss, A., Sittinger, M., & Ringe, J. (2010). Genome-wide expression profiling reveals new candidate genes associated with osteoarthritis. *YJOCA*, 18(4), 581–592.
<https://doi.org/10.1016/j.joca.2009.12.002>
- Kiyotake, E. A., Beck, E. C., & Detamore, M. S. (2016). Cartilage extracellular matrix as a biomaterial for cartilage regeneration. *Annals of the New York Academy of Sciences*, 1383(1), 139–159. <https://doi.org/10.1111/nyas.13278>
- Kong, L., Tian, Q., Guo, F., Mucignat, M. T., Perris, R., Sercu, S., ... Liu, C. (2010). Interaction between cartilage oligomeric matrix protein and extracellular matrix protein 1 mediates endochondral bone growth. *Matrix Biology*, 29(4), 276–286.
<https://doi.org/10.1016/j.matbio.2010.01.007>

- Lapointe, V. L. S., Verpoorte, A., & Stevens, M. M. (2013). *The Changing Integrin Expression and a Role for Integrin $\beta 8$ in the Chondrogenic Differentiation of Mesenchymal Stem Cells*. 8(11), 1–13.
<https://doi.org/10.1371/journal.pone.0082035>
- Lipson, K. E., Wong, C., Teng, Y., & Spong, S. (2012). *CTGF is a central mediator of tissue remodeling and fibrosis and its inhibition can reverse the process of fibrosis*. 5(Suppl 1), 2–9.
- Luo, L., Eswaramoorthy, R., Mulhall, K. J., & Kelly, D. J. (2015). Decellularization of porcine articular cartilage explants and their subsequent repopulation with human chondroprogenitor cells. *Journal of the Mechanical Behavior of Biomedical Materials*, 55, 21–31. <https://doi.org/10.1016/j.jmbbm.2015.10.002>
- Lv, F., Peng, Y., Lim, F. L., Sun, Y., Lv, M., Zhou, L., ... Leung, V. Y. L. (2016). *Matrix metalloproteinase 12 is an indicator of intervertebral disc degeneration co-expressed with fibrotic markers*. 24, 1826–1836.
<https://doi.org/10.1016/j.joca.2016.05.012>
- Mann, V., Grimm, D., Corydon, T. J., Krüger, M., Wehland, M., Riwaldt, S., ... Sundaresan, A. (2019). *Changes in Human Foetal Osteoblasts Exposed to the Random Positioning Machine and Bone Construct Tissue Engineering*.
<https://doi.org/10.3390/ijms20061357>
- Mazzoni, E., Agostino, A. D., Rosa, M., Ilaria, I., Trevisiol, L., & Charles, J. (n.d.). *Hydroxylapatite-collagen hybrid scaffold induces human adipose-derived mesenchymal stem cells to osteogenic differentiation in vitro and bone regrowth in patients*. <https://doi.org/10.1002/sctm.19-0170>
- Miao, D., Bai, X., Panda, D. K., Karaplis, A. C., Goltzman, D., & Mckee, M. D. (2004). Cartilage abnormalities are associated with abnormal Phex expression and with altered matrix protein and MMP-9 localization in Hyp mice. *BON*, 34(4), 638–647. <https://doi.org/10.1016/j.bone.2003.12.015>
- Olivares-Navarrete, R., Hyzy, S. L., Haithcock, D. A., Cundiff, C. A., Schwartz, Z., & Boyan, B. D. (2015). Coordinated regulation of mesenchymal stem cell

differentiation on microstructured titanium surfaces by endogenous bone morphogenetic proteins. *Bone*, *73*, 208–216.

<https://doi.org/10.1016/j.bone.2014.12.057>

Pei, M., Zhang, Y., Li, J., & Chen, D. (2012). Antioxidation of Decellularized Stem Cell Matrix Promotes Human Synovium-Derived Stem Cell-Based Chondrogenesis. *Stem Cells and Development*, *22*(6), 889–900.

<https://doi.org/10.1089/scd.2012.0495>

Peretti, G. M., Randolph, M. A., & Caruso, E. M. (1998). Bonding of cartilage matrices with cultured chondrocytes. *Journal of Orthopaedic Research*, *16*, 89–95.

Proteomics, Q., Of, A., To, R., & Injury, M. (2018). *QUANTITATIVE PROTEOMICS ANALYSIS OF CARTILAGE RESPONSE TO MECHANICAL INJURY AND CYTOKINE*. 11–22.

<https://doi.org/10.1016/j.matbio.2016.12.004>.QUANTITATIVE

Rangkasenee, N., Murani, E., Schellander, K., Cinar, M. U., Ponsuksili, S., & Wimmers, K. (2020). *Gene expression profiling of articular cartilage reveals functional pathways and networks of candidate genes for osteochondrosis in pigs*. (77), 856–865. <https://doi.org/10.1152/physiolgenomics.00055.2013>

Rouillard, A. D., Gundersen, G. W., Fernandez, N. F., Wang, Z., Monteiro, C. D., & Mcdermott, M. G. (2016). *Original article The harmonizome : a collection of processed datasets gathered to serve and mine knowledge about genes and proteins*. 1–16. <https://doi.org/10.1093/database/baw100>

Rowland, C. R., Colucci, L. A., & Guilak, F. (2016). Fabrication of anatomically-shaped cartilage constructs using decellularized cartilage-derived matrix scaffolds. *Biomaterials*, *91*, 57–72. <https://doi.org/10.1016/j.biomaterials.2016.03.012>

Schwarz, S., Koerber, L., Elsaesser, A. F., Goldberg-Bockhorn, E., Seitz, A. M., Dürselen, L., ... Rotter, N. (2012). Decellularized Cartilage Matrix as a Novel Biomatrix for Cartilage Tissue-Engineering Applications. *Tissue Engineering Part A*, *18*(21–22), 2195–2209. <https://doi.org/10.1089/ten.tea.2011.0705>

Seon, Y., Marjan, K., Anthony, M., & Antonios, J. M. (2019). *Applications of*

- decellularized extracellular matrix in bone and cartilage tissue engineering*. (June 2018), 83–95. <https://doi.org/10.1002/btm2.10110>
- Sztrolovics, R., Grover, J., Cs-szabo, G., Shi, S., Mort, J. S., & Roughley, P. J. (2002). *The characterization of versican and its message in human articular cartilage and intervertebral disc*. 20, 257–266.
- Taniguchi, N., Caramés, B., Kawakami, Y., Amendt, B. A., Komiya, S., & Lotz, M. (2009). *Chromatin protein HMGB2 regulates articular cartilage surface maintenance via β -catenin pathway* *AC*. 106(39), 16817–16822.
- Toh, W. S., Foldager, C. B., Pei, M., & Hui, J. H. P. (2014). *Advances in Mesenchymal Stem Cell-based Strategies for Cartilage Repair and Regeneration*. *Stem Cell Reviews and Reports*, 10(5), 686–696. <https://doi.org/10.1007/s12015-014-9526-z>
- Tomschy, A., Fauser, C., Landwehr, R., & Engel, J. (1996). *Homophilic adhesion of E-cadherin occurs by a co-operative two-step interaction of N-terminal domains*. 15(14), 3507–3514. <https://doi.org/10.1002/j.1460-2075.1996.tb00719.x>
- Tu, Y., Ma, T., Wen, T., Yang, T., Xue, L., Cai, M., ... Xue, H. (2020). *Biochemical and Biophysical Research Communications* MicroRNA-377 e 3p alleviates IL-1 b - caused chondrocyte apoptosis and cartilage degradation in osteoarthritis in part by downregulating. *Biochemical and Biophysical Research Communications*, 523(1), 46–53. <https://doi.org/10.1016/j.bbrc.2019.11.186>
- Vas, W. J., Shah, M., Blacker, T. S., Duchon, M. R., Sibbons, P., & Roberts, S. J. (2018). *Decellularized Cartilage Directs Chondrogenic Differentiation: Creation of a Fracture Callus Mimetic*. *Tissue Engineering Part A*, 24(17–18), 1364–1376. <https://doi.org/10.1089/ten.tea.2017.0450>
- Vieira, A. E., Repeke, C. E., Barros, S. De, Junior, F., Colavite, P. M., Biguetti, C. C., ... Trombone, F. (2015). *Intramembranous Bone Healing Process Subsequent to Tooth Extraction in Mice : Histomorphometric and Molecular Characterization*. 1–22. <https://doi.org/10.1371/journal.pone.0128021>
- Wang, A., Chen, M., Wang, H., Huang, J., Bao, Y., Gan, X., ... Wang, L. (2019). *Cell Adhesion-Related Molecules Play a Key Role in Renal Cancer Progression by*

Multinetwork Analysis.

- Xu, H., Xu, B., Yang, Q., Li, X., Ma, X., Xia, Q., ... Zhang, Y. (2014). Comparison of decellularization protocols for preparing a decellularized porcine annulus fibrosus scaffold. *PLoS ONE*, 9(1), 1–13. <https://doi.org/10.1371/journal.pone.0086723>
- Zhang, R., & Zhang, D. (2019). *Potential candidate biomarkers associated with osteoarthritis : Evidence from a comprehensive network and pathway analysis.* (October 2018), 17433–17443. <https://doi.org/10.1002/jcp.28365>
- Zhu, Z., Chen, G., Jiao, W. E. I., Wang, D., Cao, Y. A. N., Zhang, Q., & Wang, J. (2017). *Identification of critical genes in nucleus pulposus cells isolated from degenerated intervertebral discs using bioinformatics analysis.* 553–564. <https://doi.org/10.3892/mmr.2017.6662>